Available online at www.sciencedirect.com
ScienceDirect
Lithos 95 (2007) 177–207
LITHOS
www.elsevier.com/locate/lithos

Magmatic evolution of the Peñón Rosado granite: Petrogenesis of garnet-bearing granitoids

J.A. Dahlquist [a,*], C. Galindo [b], R.J. Pankhurst [c], C.W. Rapela [d], P.H. Alasino [a], J. Saavedra [e], C.M. Fanning [f]

[a] CRILAR-CONICET, Entre Ríos y Mendoza S/N. 5.301 Anillaco, La Rioja, Argentina
[b] Dpto. de Petrología y Geoquímica, Universidad Complutense, 28040 Madrid, Spain
[c] British Geological Survey, Keyworth, Nottingham NG125GG, UK
[d] Centro de Investigaciones Geológicas, UNLP, Calle 1 No 644, 1900 La Plata, Argentina
[e] CSIC, Instituto de Agrobiología y Recursos Naturales, 37071 Salamanca, Spain
[f] Research School of Earth Sciences, the Australian National University, Canberra, Australia

Received 30 June 2005; accepted 7 July 2006
Available online 6 September 2006

Abstract

Garnet is an uncommon accessory mineral in igneous rocks but is petrologically significant. The Peñón Rosado granite (469± 4 Ma) at Cerro Asperecito is an S-type granite that contains an unusual amount of magmatic garnet. Combined petrology, chemistry/mineralogy and whole-rock geochemistry indicates that the magma was produced by partial melting of the surrounding metasedimentary rocks and subsequent differentiation by fractional crystallization during emplacement, with garnet occurring throughout the crystallization sequence. Three facies are recognised: PRG1 (SiO_2=65.70%) represents cumulates, PRG2 (SiO_2=70.88%) represents a differentiated melt, and PRG3 (SiO_2=74.59%) a residual melt. The fractionation of Mn in garnet and the proportion of garnet crystallizing are roughly controlled by the evolving composition of the different granitic facies. Geothermobaric calculations reveal an initial crystallization temperature of 764°–792 °C and a pressure of 5.9–6.0 kb, indicating that the parental magma was emplaced at middle crustal depths (~ 19−20 km) in moderate–low magmatic temperature conditions. Major (CaO, Na_2O, K_2O) and trace element (Rb, Sr, Ba) contents in the Peñón Rosado granite strongly suggest anatexis was the outcome of H_2O-fluxed melting of metagreywacke, with heat input from a major metaluminous suite. Our studies reveal that garnet formed by direct crystallization from peraluminous magma in equilibrium with solid phases such as biotite and white mica. We confirm previous suggestions that zoning in garnet is strongly temperature-dependent. Thus, magmatic garnets in granitic rocks crystallized above ~ 700 °C have "spessartine inverse bell-shaped profile" or are unzoned, whereas garnet exhibiting "spessartine bell-shaped profile" must be considered of metamorphic origin (i.e., xenocrystic) or formed in very felsic magmas (SiO_2=73–76%) crystallizing below ~ 700 °C.
© 2006 Elsevier B.V. All rights reserved.

Keywords: S-type granite; Partial melting; Fractional crystallization; Garnet zoning

1. Introduction

Igneous garnet mostly occurs in pegmatites and aplite dykes (e.g., Leake, 1967; Manning, 1983; Deer et al., 1992), although its occurrence is also reported in some

* Corresponding author.
E-mail address: jdahlquist@crilar-conicet.com.ar (J.A. Dahlquist).

0024-4937/$ - see front matter © 2006 Elsevier B.V. All rights reserved.
doi:10.1016/j.lithos.2006.07.010

felsic to very felsic (i.e., $SiO_2 \geq 70\%$) peraluminous granitoids (e.g., Leake, 1967; Allan and Clarke, 1981; Miller and Stoddard, 1981; du Bray, 1988; Hogan, 1996; Kebede et al., 2001). Magmatic garnet is uncommon, but can help constrain host granitoid petrogenesis (du Bray, 1988) as well as being a useful geothermobarometry.

In this paper, we assess the petrography, mineral chemistry, bulk major and trace element composition, isotope ratios, and geochronology of the Peñón Rosado granite, which contains an unusual amount of garnet formed at various stages during crystallization (silica range 65.70–74.59%). Remarkably, the presence of garnet in granitic rocks of intermediate composition ($SiO_2 \sim 65.70\%$) is rare. Our study contributes to understanding granitic rocks of intermediate composition that house magmatic garnet and explain the occurrence of garnet throughout the crystallization sequence. We explore factors such as the origin of magmatic garnet, its zoning pattern, the source, initial pressure and temperature, and compositional evolution of the host magma and the overall petrogenetic process.

2. Geological setting

The Sierras Pampeanas of NW Argentina are mountainous ranges, composed of metamorphic rocks intruded by diverse Palaeozoic igneous rocks, elevated since the Miocene by compressional (Andean) tectonics (e.g., Jordan and Allmendiger, 1986) (Fig. 1). The igneous rocks were generated in three main orogenic events: (a) Pampean (latest Neoproterozoic to Mid-Cambrian), (b) Famatinian (Early to Mid-Ordovician), and (c) Achalian (Late Devonian to Early Carboniferous) (Rapela et al., 1998a,b; Pankhurst et al., 1998; Sims et al., 1998;

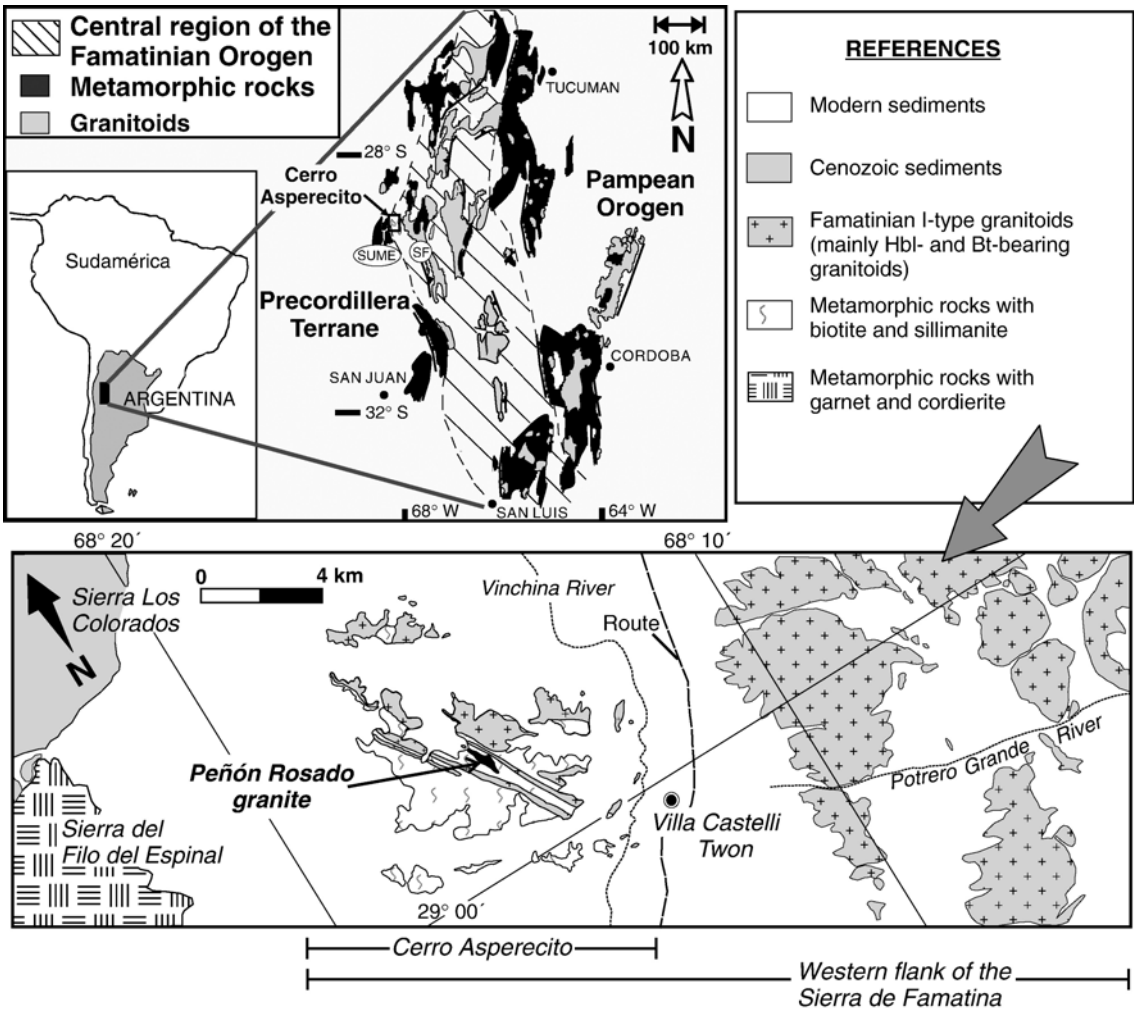

Fig. 1. Simplified geological map of Cerro Asperecito and the Peñón Rosado granite. Main inset shows location of the studied region in NW Argentina. SF = Sierra de Famatina. SUME = Sierras de Umango (west), Maz (south), and Filodel Espinal (north).

Dahlquist et al., 2005a). This study focuses on Famatinian granitoids at Cerro Asperecito in the westernmost region of the Famatinian orogen, close to the hypothetical suture between two terranes resulting from Middle Ordovician accretion (Thomas and Astini, 1996; Dalziel, 1997; Rapela et al., 1998b; Casquet et al., 2001).

The dominant plutonic rocks in this region belong to a metaluminous suite (95% of the granitic rocks at Cerro

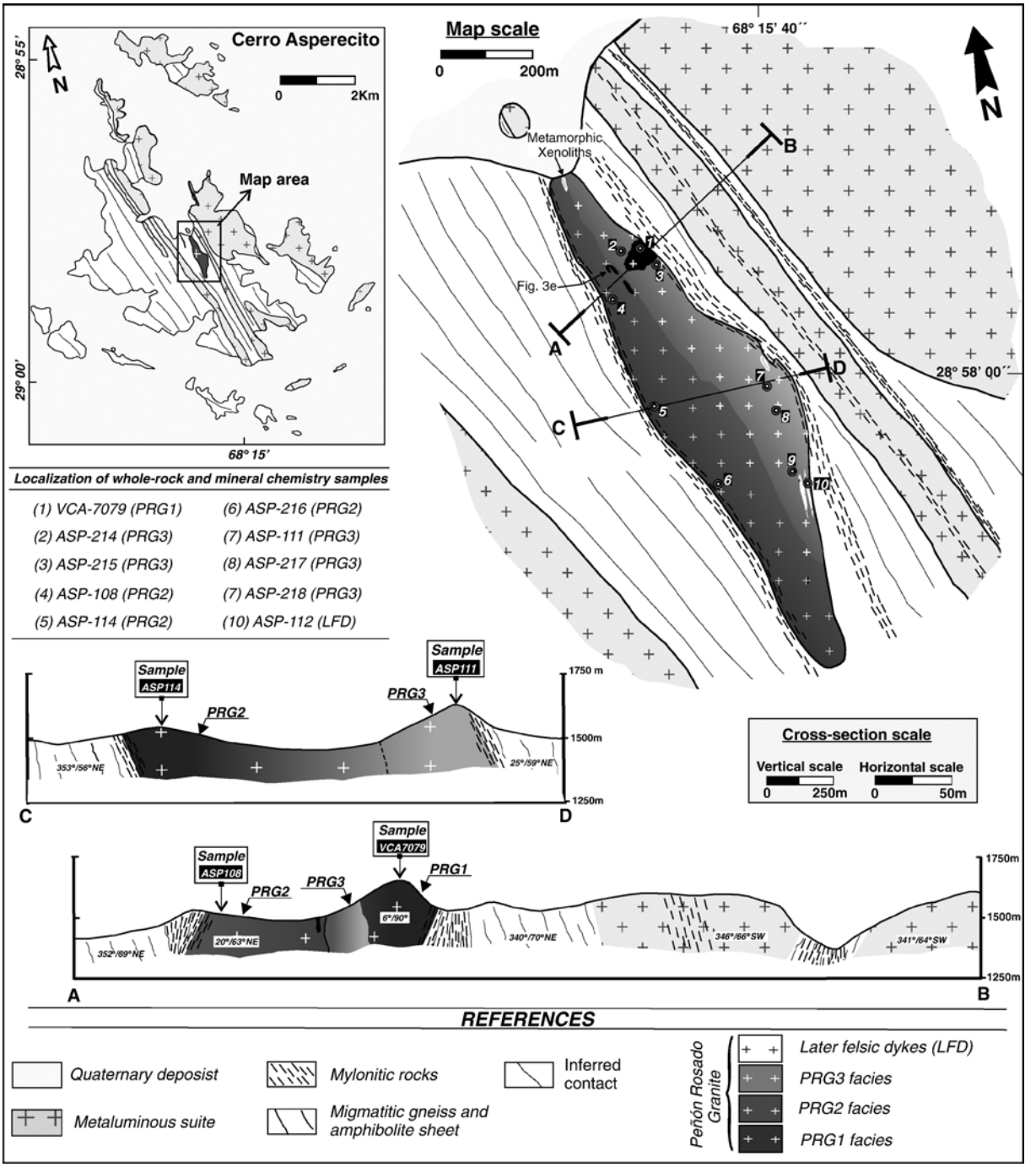

Fig. 2. Geological cross-section of the Peñón Rosado granite (PRG), showing the different lithological facies. The real size of the dykes as well as the real size of PRG1 housed in PRG2 have been magnified for its inclusion in the map.

Asperecito, Fig. 2), which range in composition from hornblende-bearing gabbro (10%) and tonalites–granodiorites (80%) to monzogranite (5%). They were emplaced in a high-grade migmatitic gneiss basement that includes biotite gneiss, biotite–sillimanite gneiss and ~ 1.5 m wide amphibolite sheets (Fig. 2). The Peñón Rosado granite is a small elongated body (0.25 km^2, Fig. 2) emplaced in the migmatitic gneisses.

The metaluminous tonalites and granodiorites are equigranular, medium-grained (1.5 cm), and white to grey in colour, typically with mafic microgranular enclaves. They are composed of Mc, Pl, Bt, and Hbl and the accessory minerals are Ep, ±Aln, Ttn, Ap, oxides, and Zrn (mineral abbreviations are taken from Kretz, 1983). The hornblende-bearing gabbro unit is equigranular, medium- to coarse-grained (1.5 cm to 5.0 cm), green-black in colour, and the magmatic association is Pl, Hbl, Qtz and Bt. The monzogranite unit is equigranular, medium-grained (1.5 cm) pink to orange in colour and consists of Mc, Pl, Qtz, Bt and Ms. Initial $^{87}Sr/^{86}Sr$ ratios and $\varepsilon(Nd)_{468}$ (average of three samples) are 0.70886 and −5.1 (Dahlquist and Galindo, 2004). It is suggested that the parental melt of the metaluminous suite was mainly derived by melting of meta-igneous rocks in the middle to lower crust, without asthenospheric mantle contamination, a common feature of the metaluminous Famatinian granitoids. Geochronological data indicate that major metaluminous suite was emplaced during the Middle Ordovician (468 Ma, Pankhurst et al., 2000), almost synchronously with the Peñón Rosado granite (469 Ma, this work) and in similar *P–T* conditions ($T=763\pm30$ °C, $P=4.7\pm0.5$ kb; Dahlquist et al., 2006 and this work).

3. The Peñón Rosado granite: petrology, mineral chemistry and whole-rock geochemistry

3.1. Analytical methods

Petrographic investigations were conducted on 25 samples of the Peñón Rosado granite. Whole-rock major and trace elements were determined for 10 representative samples of the granite and 1 felsic dyke using ICP and ICP-MS (following the procedure 4-lithoresearch code), at Activation Laboratories, Ontario, Canada (ACTLABS).

Mineral chemistry was determined using a JEOL Superprobe JXA-8900-M equipped with five crystal spectrometers at the Luis Brú Electron Microscopy Center, Complutense University, Madrid, Spain. Operating conditions were: acceleration voltage of 15 kV, probe current of 20 nA, with a beam diameter between 1 to 2 μm. Absolute abundances for each element were determined by comparison with standards (Jarosewich et al., 1980; McGuire et al., 1992). An on-line ZAF program was used.

Rb–Sr and Sm–Nd determinations of four samples were carried out at the Geochronology and Isotope Geochemistry Center of the Complutense University (Madrid, Spain). Isotopic analyses were made on an automated multicollector VG® SECTOR 54 mass spectrometer. Errors are quoted throughout as two standard deviations from measured or calculated values. Analytical uncertainties are estimated to be 0.01% for $^{87}Sr/^{86}Sr$, 0.006% for $^{143}Nd/^{144}Nd$, 1% for $^{87}Rb/^{86}Sr$, and 0.1% $^{147}Sm/^{144}Nd$. Replicate analyses of the NBS-987 Sr-isotope standard yielded an average $^{87}Sr/^{86}Sr$ ratio of 0.710247 ± 0.00003 ($n=524$). Fifty six analyses of La Jolla Nd-standard over year gave a mean $^{143}Nd/^{144}Nd$ ratio of 0.511846 ± 0.00003.

3.2. Field occurrence and macroscopic description

The Peñón Rosado granite is emplaced parallel to ~ N–S structural trends (350°–340°) in the high-grade migmatitic gneiss terrane (Figs. 2 and 3a), of which it contains large xenoliths (Fig. 3b). The metaluminous suite crops out on both sides of the granite and both contacts have a superimposed mylonitic foliation, which is also observed in the metamorphic basement (~ 350°, Fig. 3c). The main dip of the metamorphic basement foliation is NE (59° to 69°), although at the contacts this changes to SW with a higher angle (81°, Fig. 2), suggesting that the dip variation is due to the differential distribution of the mylonitic event on two bodies with distinctive rheological properties, the granitic rocks being more rigid than the metamorphic rocks.

The Peñón Rosado granite is massive, but in some places exhibits mineral alignment defining a single mylonitic foliation. Generally, it is leucocratic to mesocratic, containing biotite and subordinate muscovite. Based on field, petrographic and geochemical data, three facies are recognised: PRG2 and PRG3 are dominant, whereas PRG1 is subordinate, forming a very small outcrop (Fig. 2). All facies of the Peñón Rosado granite are medium-grained (0.5 cm), inequigranular, and with uniformly distributed 1- to 2-cm phenocrysts of garnet (Fig. 3d). A garnet count was carried out in the field using 400 cm^2 grids (four per facies), revealing an average of 25 grains for PRG1, 21 grain for PRG2, and 23 grains for PRG3.

Thin late felsic dykes (50–60 cm width and 100–150 cm length) of medium-grain size (0.4 cm) and with a structural trend of 3°/90° are included in the PRG3

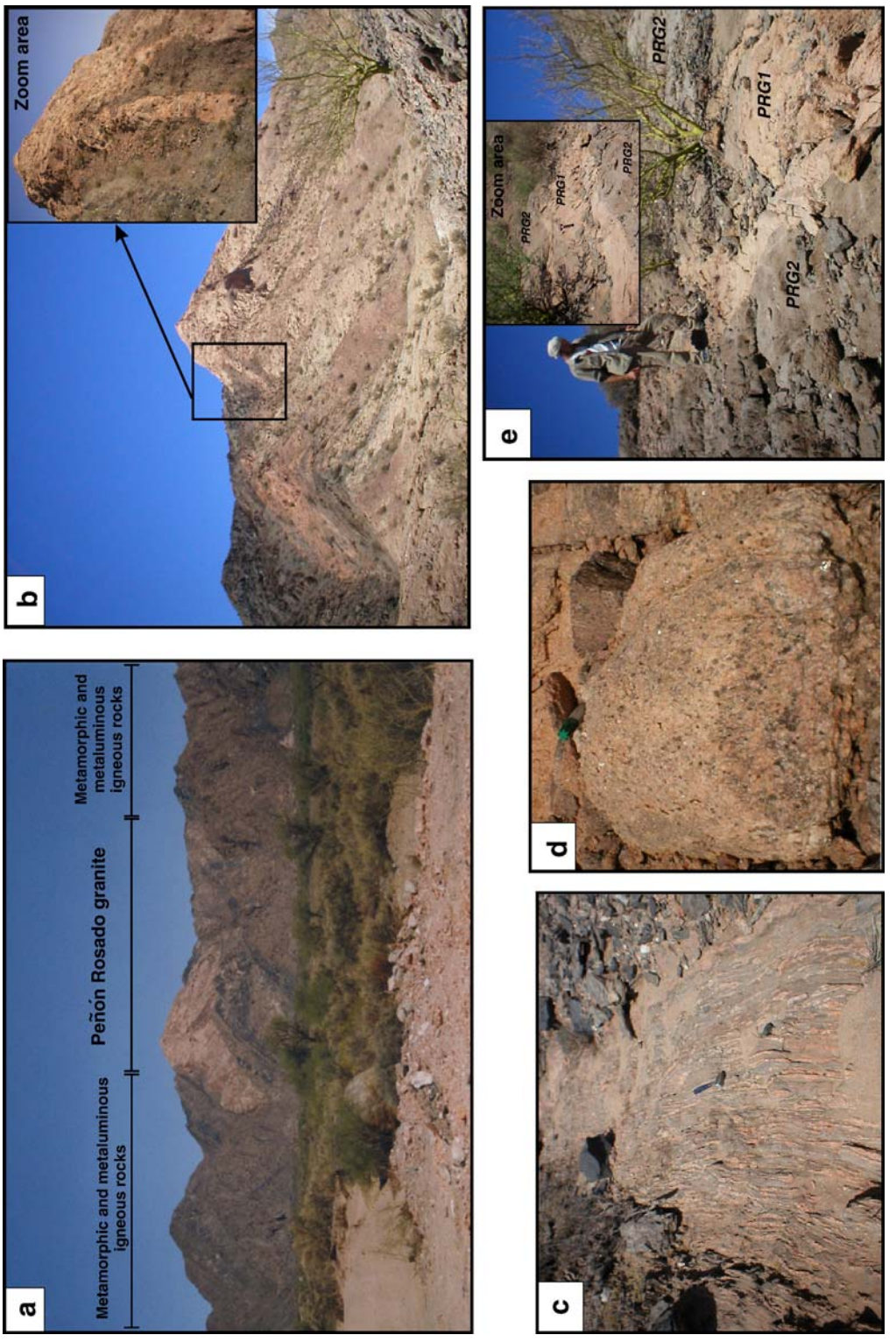

Fig. 3. Field characteristics of the Peñón Rosado granite. (a) Panoramic scene of the outcrop. (b) Intrusion into migmatitic gneiss. (c) Migmatitic gneiss with mylonitic deformation. (d)Equigranular granite (PRG3) with homogeneously distributed garnet megacrysts (black dots). (e) Fragment of the facies PRG1 in PRG2 in the contact area. A sharp contact is observed between both facies.

facies (Fig. 2) and consist of Pl, Qtz and Grt. The PRG1 facies is leucocratic, pink-to-orange, with very high Pl content (64.37%) and subordinate Grt, Bt and Ms. PRG2 is mesocratic, grey, with Pl, Qtz, Grt and abundant Bt and Ms. PRG3 is leucocratic, pink-to-orange, with Pl, Grt, Bt, Ms, and abundant Kfs and Qtz. The presence of small rectangular to irregular fragments (2.5 m × 1.5 m or 5 m × 1 m) of the PRG1 facies in PRG2 (Fig. 3e), and the disruption of PRG1 by PRG2 in the contact area, suggest that the PRG2 facies was introduced when PRG1 was solid or partially molten.

3.3. Petrography and mineral chemistry

The magmatic assemblage for all three facies of the Peñón Rosado granite is Pl–Qtz–Kfs–Bt–Ms–Grt, with Zrn and oxides (mainly magnetite and hematite after magnetite) as accessory minerals. However, mineral proportions are very different in each facies (Table 1). Fluorapatite (with F = 3.35% and CaO = 54.32%; analyses from one sample) and monazite were observed in PRG2. All the facies contain a very low percentage of oxides (0.2–0.4%), which can even be absent in PRG1 and PRG3. Secondary epidote and biotite mantled by chlorite (after biotite) is common in PRG1. Analysed chlorites have high MnO contents (average of 5 samples = 2.41%). Quartz forms anhedral crystals and in PRG3 occurs both in the framework of the rock and as inclusions in alkali feldspar. Undulose extinction is observed in all the quartz.

3.3.1. Plagioclase

Two main varieties of plagioclase were recognized in PRG1: (a) Pl_a (3.2 × 1.9 mm), with patchy zoning, forming tabular and anhedral crystals and (b) Pl_b (1.7 × 0.9 mm), with continuous zoning, forming tabular, subhedral crystals with polysynthetic twinning. A fine-grained Pl_c (0.6 × 0.4 mm) occasionally appears in PRG1. The patchy zoning in Pl_a is formed by intergrowth between a Na-rich phase ($Ab_{69.2}$ $An_{29.1}$ $Or_{1.6}$) and Ca-rich phase ($Ab_{66.5}$ $An_{32.3}$ $Or_{1.2}$; Table 2a). Pl_b compositions range from $Ab_{66.1}$ $An_{33.0}$ $Or_{0.9}$ in the core to $Ab_{67.8}$ $An_{31.3}$ $Or_{0.9}$ in the rim (Table 2a). Two varieties of plagioclase, were also recognized in PRG2 (Pl_a, 2.8 × 1.9 mm and Pl_b, 1.8 × 1.1 mm) with similar features to the Pl_b in PRG1. The composition range is from $Ab_{58.5}$ $An_{39.8}$ $Or_{1.7}$ in the core to $Ab_{64.2}$ $An_{34.2}$ $Or_{1.6}$ in the rim for Pl_a; and $Ab_{52.1}$ $An_{46.4}$ $Or_{1.4}$ in the core to $Ab_{62.3}$ $An_{35.8}$ $Or_{1.9}$ in the rim for Pl_b (Table 2a). The plagioclase in PRG3 facies occurs in two sizes, medium-grained (Pl_a, 2.8 × 1.3 mm) and fine-grained (Pl_b, 1.2 × 0.6 mm). Both form tabular subhedral–anhedral crystals with polysynthetic twinning and continuous zonation. Pl_a shows an oscillatory profile from $Ab_{80.4}$ $An_{18.0}$ $Or_{1.60}$ to $Ab_{82.2}$ $An_{16.1}$ $Or_{1.70}$ (Table 2a).

3.3.2. Alkali feldspar

In PRG1 interstitial alkali feldspar (Mc) occasionally appears filling small cavities in deformed plagioclase crystals (curved twinning and fracture). The alkali feldspar in PRG2 occurs sparsely as individual grains of

Table 1
Modal and chemical classification of Peñón Rosado granite

Igneous facies	PRG1	PRG2	PRG3	LFD
Representative samples	VCA-7079 $n=2$	ASP-114 $n=1$	ASP-111 $n=1$	ASP-112 $n=1$
Total points	*1640*	*926*	*1027*	*934*
Qtz	24.9±4.6	32.8	33.2	45.5
Kfs	Tr	7.8	25.6	–
Pl	64.2±3.0	45.7	34.4	52.5
Bt	5.4±0.7	11.0	1.2	0.6
Ms	2.2±0.1	1.0	2.7	0.3
Grt	1.8±0.1	0.5	1.5	0.9
Ap	–	0.2	–	–
Zrn	0.3±0.1	0.2	0.2	–
Mnz	–	0.3	–	–
Mag	0.3±0.1	0.4	0.3	0.2
Chl + Ep	0.9±0.4	0.1	–	–
Modal classification QAP[a]	*Tonalite*	*Tonalite–granodiorite*	*Monzongranite*	*Tonalite*
Ab–An–Or[b]	*Trondhjemite*	*Tonalite–granodiorite*	*Granite*	*Trondhjemite*

Nomenclature in the table: Abbreviation mineral taken from Kretz (1983). Abbreviations: PRG: Peñón Rosado granite; LFD: late felsic dyke; Tr = traces; n = number of samples. Dashed line: absent mineral.

[a] QAP classification following Streckeisen (1976).

[b] Ab–An–Or classification following Barker (1979). Chemical data in Table 3.

Table 2a
Representative compositions of plagioclases in Peñón Rosado granite from electron microprobe analyses

Igneous facies	PRG1	PRG1	PRG1	PRG1	PRG1	PRG1
Sample	VCA-7079	VCA-7079	VCA-7079	VCA-7079	VCA-7079	VCA-7079
Analysis number	63	64	65	Av. (n=4)	Av. (n=2) core zone	Av. (n=2) rim zone
Mineral	Pl_a (patchy zoning)			Pl_b[a]	Pl_b	Pl_b
wt.%						
SiO_2	59.33	60.11	60.23	59.42±0.42	59.29±0.14	59.73±0.28
TiO_2	bdl	bdl	0.07	bdl	bdl	bdl
Al_2O_3	24.85	25.09	25.09	25.07±0.23	25.23±0.22	24.91±0.09
FeO	0.06	0.02	0.01	0.06±0.05	0.03±0.03	0.06±0.05
MnO	bdl	0.02	bdl	0.02±0.02	0.04±0.03	0.03±0.02
MgO	0.02	bdl	bdl	bdl	bdl	bdl
CaO	5.96	6.83	6.67	6.70±0.15	6.97±0.03	6.61±0.07
Na_2O	7.83	7.73	7.59	7.77±0.16	7.72±0.03	7.90±0.03
K_2O	0.28	0.15	0.22	0.18±0.08	0.16±0.04	0.16±0.07
Total	98.34	99.97	99.91	99.25±0.52	99.42±0.27	99.39±0.30
Ab	69.20	66.60	66.50	67.05	66.11	67.76
An	29.10	32.50	32.30	31.94	32.98	31.33
Or	1.60	0.90	1.20	1.02	0.91	0.91

Igneous facies	PRG2	PRG2	PRG2	PRG2
Sample	ASP-114	ASP-114	ASP-114	ASP-114
Analysis number	Av. (n=2) core zone	Av. (n=3) rim zone	43 core zone	Av. (n=2) rim zone
Mineral	Pl_a		Pl_b	
wt.%				
SiO_2	58.04±0.13	59.25±0.31	56.41	58.38±0.01
TiO2	0.01±0.01	bdl	bdl	bdl
Al_2O_3	26.59±0.00	25.58±0.21	27.64	25.53±0.16
FeO	0.02±0.01	0.06±0.05	0.05	0.06±0.02
MnO	0.04±0.01	0.03±0.03	0.03	bdl
MgO	0.02±0.03	0.01±0.00	bdl	bdl
CaO	8.22±0.03	7.19±0.12	9.54	7.43±0.12
Na_2O	6.68±0.10	7.46±0.02	5.92	7.14±0.01
K_2O	0.30±0.01	0.28±0.04	0.25	0.33±0.02
Total	99.92±0.21	99.86±0.24	99.84	98.84±0.30
Ab	58.5	64.21	52.10	62.29
An	39.76	34.2	46.40	35.82
Or	1.74	1.59	1.40	1.89

Igneous facies	PRG3	PRG3	PRG3	PRG3
Sample	ASP-111	ASP-111	ASP-111	ASP-111
Analysis number	140 rim zone	141 core zone	142 core zone	143 rim zone
Mineral	Oscillatory zoning Pl_a			
wt.%				
SiO_2	63.93	63.73	63.81	62.825
TiO_2	0.01	bdl	bdl	bdl
Al_2O_3	22.63	22.81	22.19	23.014
FeO	bdl	0.04	0.04	bdl
MnO	0.07	bdl	bdl	bdl
MgO	bdl	bdl	bdl	0.02
CaO	3.37	3.66	3.49	3.79
Na_2O	9.51	9.47	9.33	9.37
K_2O	0.30	0.28	0.39	0.29

(continued on next page)

Table 2a (*continued*)

Igneous facies	PRG3	PRG3	PRG3	PRG3
Sample	ASP-111	ASP-111	ASP-111	ASP-111
Analysis number	140 rim zone	141 core zone	142 core zone	143 rim zone
Mineral	Oscillatory zoning Pl_a			
wt.%				
Total	99.81	100.01	99.26	99.29
Ab	82.20	81.10	81.00	80.40
An	16.10	17.30	16.80	18.00
Or	1.70	1.60	2.20	1.60

Igneous facies	LFD	LFD	LFD	LFD	LFD	LFD
Sample	ASP-112	ASP-112	ASP-112	ASP-112	ASP-112	ASP-112
Analysis number	Av. (n=2)	17 rim zone	18 between 17–19	19 core zone	20 between 19–21	21 rim zone
Mineral	Pl_a	Oscillatory zoning Pl_b				
wt.%						
SiO_2	60.80±0.02	61.02	62.50	61.63	61.31	60.88
TiO_2	0.02±0.02	0.00	0.00	0.00	0.00	0.01
Al_2O_3	23.98±0.23	23.45	22.86	23.31	23.70	23.83
FeO	0.01±0.01	0.00	0.05	0.03	0.02	0.02
MnO	0.04±0.01	0.01	0.00	0.00	0.00	0.00
MgO	bdl	0.01	0.01	0.00	0.01	0.00
CaO	5.96±0.02	5.19	3.98	4.74	4.42	5.42
Na_2O	8.38±0.04	8.61	8.90	8.59	8.14	8.47
K_2O	0.25±0.01	0.21	0.41	0.24	0.46	0.23
Total	99.43±0.22	98.51	98.71	98.54	98.06	98.86
Ab	70.8	74.10	78.30	75.60	74.80	72.90
An	27.82	24.70	19.30	23.00	22.40	25.80
Or	1.39	1.20	2.30	1.40	2.80	1.30

Nomenclature in the table: Total iron measured as FeO, structural formulae calculated following Richard (1995), mineral abbreviation are taken from Kretz (1983). Abbreviations: PRG=Peñón Rosado granite; bdl=below detection limit; Av.=average; n=number of samples.
References as in Table 2a for the plagioclases in PRG1.
LFD=Late felsic dyke.
[a] Representative composition of plagioclase used in geothermobarometry and fractional crystallization model using major oxides, which result from the average between core and rim zone of the Pl_b (explanation in Section 7).

orthoclase (representative composition in Table 2b). The lack of cross-hatched twinning and microperthite suggests crystallization in the upper solvus field, and a very low Na content in the magma during the crystallization of PRG2. Mc is abundant in PRG3 (Table 1), is coarse-to-medium-grained (Mc_a, 5.1×3.3 mm to 2.6×1.3 mm), and forms rectangular subhedral–anhedral crystals, generally with perthitic texture and inclusions of Qtz–Pl–Ms. The medium-to-fine-grained Mc_b (0.6×0.3 mm) is intergranular and without inclusions. A representative composition of Mc_a is shown in Table 2b.

3.3.3. Garnet

Garnet is abundant in all facies of the Peñón Rosado granite and is present in most of the collected samples (Table 1). All garnets types have distinctive red cores, with hematite(?)-coated fractures and form hexagonal sections, some time irregular, euhedral to subhedral crystals without or few mineral inclusions such as chlorite (after biotite) and secondary muscovite. Fig. 4 shows that garnet compositions in the Peñón Rosado granite are similar to those in other peraluminous plutons and, in particular, to the magmatic garnets reported by du Bray (1988). In the PRG, the textural studies have revealed three garnet populations according to their sizes in PRG1: Grt_a (1.7–1.5 mm), Grt_b (1.3–1.0 mm) and Grt_c (0.8–0.6 mm); two garnet populations in PRG2: Grt_a (2.3×1.9 mm), Grt_b (1.7×1.0 mm), and a single garnet population in PRG3 (Grt_a, 2.1×2.2 mm). The analysed garnets in PRG are largely a solid solution of almandine–spessartine, which constitutes 81.32–88.53% of the total molecular composition (Table 2c). Pyrope, andradite, and grossular, and very rare or absent uvarovite, together make up the remainder. Detailed petrographic and electron microprobe studies revealed

Table 2b
Representative compositions of alkali feldspar in Peñón Rosado granite from electron microprobe analyses

Igneous facies	PRG2	PRG2	PRG3	PRG3	PRG3	PRG3
Sample	ASP-114	ASP-114	ASP-111	ASP-111	ASP-111	ASP-111
Analysis number	47	50	2 rim zone	3 central zone	4 central zone	5 rim zone
Mineral	Kfs	Kfs	Kfs			
wt.%						
SiO_2	64.16	63.87	64.08	64.30	63.32	63.86
TiO_2	0.01	bdl	0.03	bdl	0.02	0.02
Al_2O_3	18.85	18.77	18.72	18.61	18.79	18.51
FeO	0.02	bdl	bdl	0.04	bdl	bdl
MnO	0.05	bdl	bdl	bdl	0.03	bdl
MgO	bdl	bdl	bdl	0.03	0.01	bdl
CaO	0.07	0.05	0.05	0.042	0.04	0.10
Na_2O	1.11	0.91	1.58	1.51	1.30	1.40
K_2O	15.37	15.25	15.80	15.47	15.84	15.59
Total	99.64	98.85	100.31	100.08	99.41	99.52
Ab	9.90	8.30	13.10	12.90	11.10	11.90
An	0.30	0.30	0.20	0.20	0.20	0.50
Or	89.80	91.50	86.60	86.90	88.70	87.60

References as in Table 2a for the plagioclases in PRG1.

that all the garnet types in each facies have a similar zoning pattern and similar absolute oxides concentrations. Two garnets housed in the PRG1 were chosen for compositional mapping and zoning profiles (Fig. 5 and Table 2c). A spessartine component between 27.86 and 30.29% (average from 9 samples = 28.96%) is representative of the large unzoned homogenous central area, whereas the marginal rims typically have 34.69–43.50% (average from 8 samples = 39.18%). The intermediate compositional zone has a spessartine range between 32.11 and 33.38% (average from 4 samples = 33.21%). Thus, the profiles exhibited relatively Mn-poor central

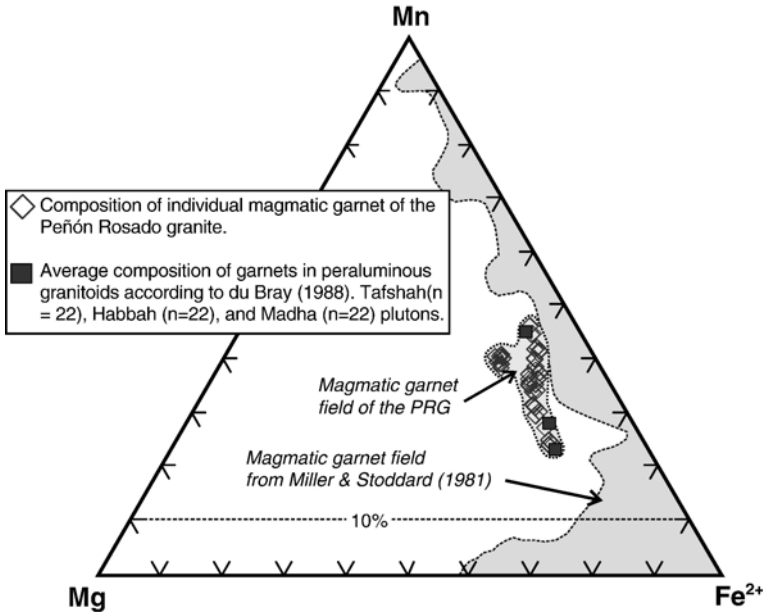

Fig. 4. Garnet compositions (Mn, Fe, and Mg) for the Peñón Rosado granite. The grey field is for garnet compositions from the compilation of Miller and Stoddard (1981) and garnet compositions in peraluminous granitoids are from du Bray (1988). The compilation of Miller and Stoddard (1981) reveals that an overwhelming majority of garnets found in granitoids contain >10% spessartine component (n = number of analyses).

Table 2c
Representative compositions of garnet in Peñón Rosado granite from electron microprobe analyses

Igneous facies	PRG1	PRG1	PRG1	PRG1	PRG1	PRG1	PRG1	PRG1	PRG1	PRG1
Sample	VCA-7079	VCA-7079	VCA-7079	VCA-7079	VCA-7079	VCA-7079	VCA-7079	VCA-7079	VCA-7079	VCA-7079
Analysis number	Av. (n=7) CZ[a]	Av. (n=2) ICZ	Av. (n=4) MRZ	1 MRZ	2 MRZ	29 ICZ	3 RC	4 RC	6 MRZ	7 MRZ
Mineral	Grt_a			Composition profile Grt_a						
wt.%										
SiO_2	37.58±0.17	37.68±0.18	37.12±0.14	37.11	37.55	37.80	37.85	37.37	36.94	37.13
TiO_2	0.09±0.09	bdl	0.02±0.02	0.02	bld	bld	0.02	0.23	0.06	bdl
Al_2O_3	21.16±0.26	21.47±0.14	21.5±0.18	21.43	21.57	21.37	21.50	20.99	21.68	21.62
FeO	23.96±0.58	22.04±1.1	20.72±0.87	20.78	21.27	22.82	24.31	24.50	21.90	20.28
CFeO	23.96	22.04	20.72	20.78	21.27	22.82	24.31	23.99	21.90	20.28
CFe_2O_3	0.00	0.00	0.00	0.00	0.00	0.00	0.00	0.57	0.00	0.00
MnO	12.78±0.32	14.3±0.01	16.66±0.75	17.00	14.29	14.31	12.75	12.37	15.57	16.82
MgO	3.44±0.09	2.71±0.34	2.2±0.43	1.98	2.47	2.94	3.31	3.51	2.80	1.81
CaO	1.45±0.22	1.28±0.07	1.43±0.19	1.43	1.23	1.33	1.40	1.61	1.20	1.66
Na_2O	0.02±0.02	0.01±0.01	0.01±0.01	0.01	bld	0.03	bld	0.04	0.02	0.01
K_2O	bdl	bdl	bdl	bld	bld	bld	bld	bld	bld	bld
Total	100.48	99.49	99.67	99.76	98.38	100.60	101.14	100.62	100.17	99.33
CTotal	100.48	99.49	99.67	99.76	98.38	100.60	101.14	100.68	100.17	99.33
End-members calculated following Deer et al. (1992)										
Almandine	53.32	51.24	47.78	47.91	50.97	51.48	54.14	53.46	49.51	47.52
Andradite	0.00	0.00	0.00	0.00	0.00	0.00	0.00	1.55	0.00	0.00
Grossular	4.13	3.81	4.22	4.22	3.77	3.85	3.98	3.03	3.49	4.97
Pyrope	13.65	11.23	9.04	8.13	10.54	11.84	13.14	13.91	11.28	7.54
Spessartine	28.80	33.67	38.91	40.00	34.69	32.69	28.75	27.86	35.65	39.91
Uvarovite	0.00	0.00	0.00	0.00	0.02	0.00	0.00	0.00	0.00	0.00

Igneous facies	PRG1	PRG1	PRG1	PRG1	PRG1	PRG1	PRG1	PRG1
Sample	VCA-7079	VCA-7079	VCA-7079	VCA-7079	VCA-7079	VCA-7079	VCA-7079	VCA-7079
Analysis number	8 MRZ	9 MRZ	15 ICZ	10 RC	11 RC	14 ICZ	12 MRZ	13 MRZ
Mineral	Composition profile Grt_b							
wt.%								
SiO_2	36.94	37.26	37.83	37.36	37.41	37.78	37.89	37.41
TiO_2	0.01	bdl	0.01	bdl	0.08	0.01	0.06	bdl
Al_2O_3	21.37	21.21	21.62	21.78	21.52	21.40	21.76	21.27
FeO	19.72	22.20	23.29	23.83	23.61	22.70	22.01	19.17
CFeO	19.72	22.20	23.29	23.83	23.61	22.70	22.01	19.17
CFe_2O_3	0.00	0.00	0.00	0.00	0.00	0.00	0.00	0.00
MnO	18.10	15.40	14.32	12.92	13.06	14.72	16.06	18.46
MgO	1.76	2.34	2.89	3.30	3.35	2.76	2.38	1.68
CaO	1.40	1.67	1.74	1.31	1.33	1.62	1.50	1.61
Na_2O	0.01	0.01	bdl	bdl	0.02	0.03	0.02	0.02
K_2O	bdl	bdl	bdl	bdl	bdl	bdl	bdl	bdl
Total	99.31	100.08	101.71	100.50	100.35	101.02	101.59	99.61
CTotal	99.31	100.08	101.71	100.50	100.35	101.02	101.59	99.61
End-members calculated following Deer et al. (1992)								
Almandine	45.84	50.30	51.55	53.58	52.97	50.82	49.49	44.61
Andradite	0.00	0.00	0.00	0.00	0.00	0.00	0.00	0.00
Grossular	4.18	4.83	4.93	3.78	3.82	4.66	4.32	4.80
Pyrope	7.30	9.43	11.41	13.22	13.40	11.01	9.53	6.98
Spessartine	42.63	35.34	32.11	29.42	29.68	33.38	36.58	43.50
Uvarovite	0.00	0.03	0.00	0.00	0.00	0.00	0.00	0.00

Table 2c (*continued*)

Igneous facies	PRG1	PRG1	PRG2	PRG2	PRG3	LFD	LFD
Sample	VCA-7079	VCA-7079	ASP-114	ASP-114	ASP-111	ASP-112	ASP-112
Analysis number	Av. (n=3) CZ	Av. (n=2) RZ	Av. (n=3) CZ	55RZ	Av. (n=9) CRZ	Av. (n=3) CZ	Av. (n=2) RZ
Mineral	Grt_c		Grt_a		Grt	Grt	
wt.%							
SiO_2	37.24±0.12	37.21±0.33	37.65±0.13	38.05	37.21±0.34	37.25±0.10	37.04±0.12
TiO_2	bdl	0.15±0.05	0.05±0.04	0.02	0.07±0.04	0.05±0.07	0.02±0.02
Al_2O_3	21.22±0.30	21.24±0.15	21.56±0.19	21.88	21.25±0.36	21.47±0.24	21.53±0.00
FeO	23.26±0.15	19.85±0.32	26.12±0.11	25.50	19.60±0.36	22.52±0.47	21.13±0.06
CFeO	23.26±0.15	19.85±0.32	23.12±0.11	25.50	19.49±0.32	22.42±0.32	21.13±0.06
CFe_2O_3	0.00	0.00	0.00	0.00	0.18±0.28	0.12±0.16	0.00
MnO	13.43±0.18	17.60±0.40	10.17±0.20	11.61	16.93±0.32	14.52±0.28	16.56±0.26
MgO	2.81±0.15	1.61±0.15	3.55±0.10	3.39	3.66±0.16	3.00±0.06	2.04±0.17
CaO	1.42±0.15	1.57±0.06	1.39±0.03	1.25	0.70±0.10	1.16±0.07	1.14±0.06
Na_2O	0.01±0.01	bdl	0.02±0.01	0.02	0.03±0.02	0.03±0.03	0.00
K_2O	bdl	bdl	bdl	0.01	0.00	0.01±0.01	0.00
Total	99.40±0.49	98.98±0.53	100.54±0.13	101.76	99.53±0.42	100.00±0.26	99.44±0.06
CTotal	99.40±0.49	98.98±0.53	100.54±0.13	101.76	99.55±0.41	100.02±0.29	99.44±0.06
End-members calculated following Deer et al. (1992)							
Almandine	53.21	46.64	58.60	56.74	44.2	50.84	49.10
Andradite	0.00	0.00	0.00	0.00	0.49	0.25	0.00
Grossular	4.16	4.73	4.00	3.55	1.52	3.13	3.40
Pyrope	11.46	6.74	14.20	13.46	14.79	12.16	8.50
Spessartine	31.12	41.89	23.11	26.16	38.82	33.45	39.0
Uvarovite	0.00	0.00	0.00	0.00	0.00	0.00	0.00

References as in Table 2a for the plagioclases in PRG1. Total iron measured as FeO; Fe^{3+} calculated following Droop (1987); C=calculated. CZ=central zone; IRZ=intermediate compositional zone; MRZ=marginal rim zone.

Averaged samples in: CZ=3, 4, 30, 31, 32, 33, 34; ICZ=29, 2; MRZ=1, 6, 7, 35. All samples in Fig. 5.

References as in Table 2a for the plagioclases in PRG1. Total iron measured as FeO; Fe^{3+} calculated following Droop (1987); C=calculated. LFD=late felsic dyke. CZ=central zone; CRZ=central-rim zone; RZ=rim zone.

[a] Representative composition of garnet used in geothermobarometry and fractional crystallization model using major oxides, which result from the average of the central zone (explanation in Section 7).

zones and relatively Mn-rich marginal rims zones, constituting a "spessartine inverse bell-shaped profile" (Fig. 5). In addition, Mn vs. Fe^{2+}+Mg shows inverse correlation from marginal rim to central zone (Table 2c). The MnO content in the PRG2 garnets is lower than in PRG1 garnets but the FeO content is slightly higher. The characteristic zoning pattern exhibits a relatively Mn-poor central zone and a relatively Mn-rich rim zone, but with narrow composition variation (Table 2d), constituting a "smooth spessartine inverse bell-shaped profile". The PRG3 garnets have the highest MnO contents of any in the pluton. These garnets have relatively homogeneous spessartine content, with very narrow compositional variation (from spessartine 37.49% in the core to 39.72% in the rim, Table 2d), and are thus essentially unzoned.

3.3.4. Dark micas

The black micas in PRG1 and PRG2 occur in two sizes, medium-grained (Bt_a, 1.4×0.6 mm) and fine-grained (Bt_b, 0.5×0.3 mm), whereas the biotites in PRG3 are fine-grained (0.3×0.2 mm). All form tabular and irregular sections, are subhedral, and have light to dark brown pleochroism. Oxides, Ap and Zrn occur as inclusions in the PRG1 and PRG2 black micas, whereas zircon inclusions were observed in PRG3. The PRG1 black micas are commonly chloritized. In terms of Al^{IV} vs. $Fe^{2+}/(Fe^{2+}+Mg)$ the black micas of the Peñón Rosado granite are classified as biotites with high siderophyllite–eastonite contents (Table 2d). The biotites in PRG3 have a similar composition to those in PRG1 and PRG2, although the $Fe^{2+}/(Fe^{2+}+Mg)$ ratios are slightly lower (Table 2d).

The biotites of all facies have consistently high Al^{IV} (mean 2.48 to 2.64 atom/formula unit) together with high MnO contents (e.g., 0.85% in the PRG1 facies, Table 2d), as found by Miller and Stoddard (1981) for biotite in garnet-bearing granite. Biotites with high Al^{IV} seem to be characteristic of peraluminous granites (e.g., Dahlquist et al., 2005b; Clarke et al., 2005) where they coexist with aluminous minerals (Table 2d).

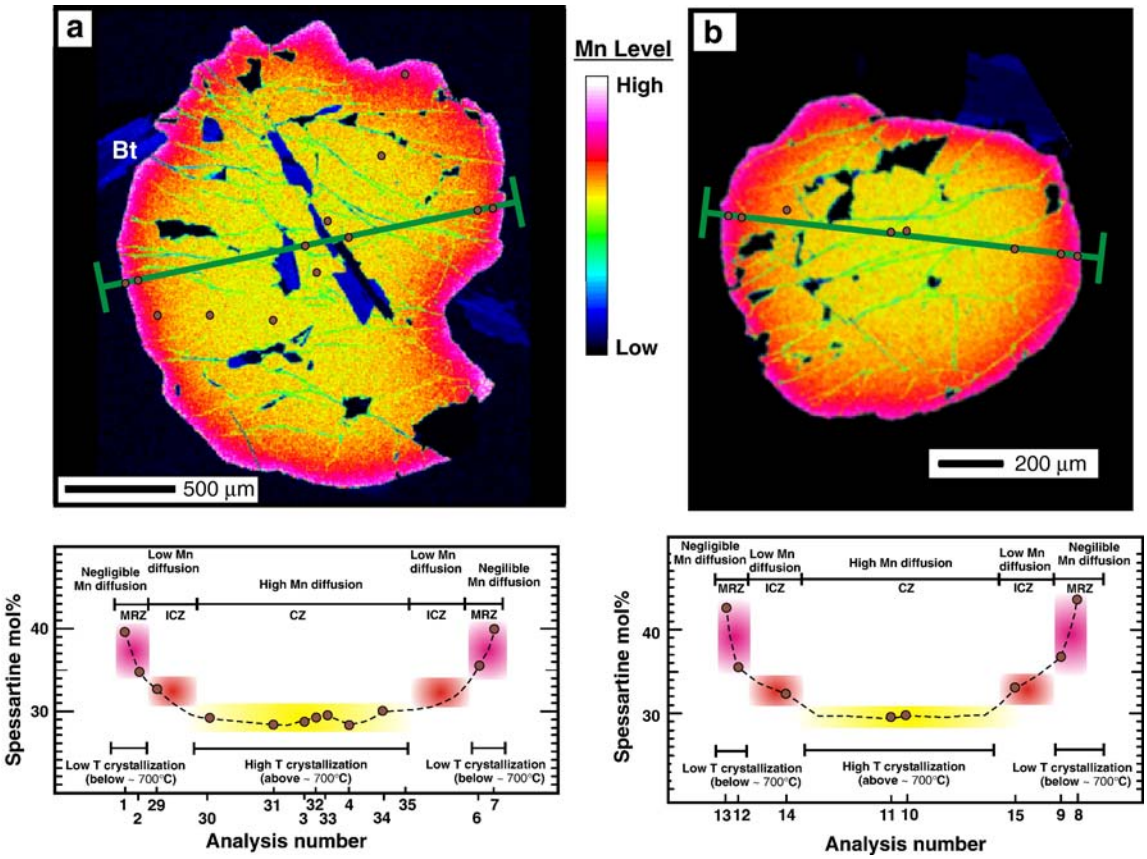

Fig. 5. X-ray compositional maps and zoning profiles for spessartine content from sample VCA-7079 (PRG1 facies) using electron microprobe. In general, the spessartine content follows an inverse bell-shaped profile. There is a large homogenous central zone (spessartine average = 28.96%), an intermediate compositional zone (spessartine average = 33.21%) and Mn enrichment of marginal rims (spessartine average = 39.18%). Orientations of the compositional profiles are indicated on the garnet. CZ = central zone, ICZ = intermediate compositional zone, and MRZ = marginal rim zone. Data in Table 2c.

3.3.5. White micas

White mica is the other sheet silicate present. Care was taken to determine whether it is of primary or secondary origin, since primary white mica is widely held to be an indicator of peraluminous magmas (Speer, 1984). Petrographic observations using the criteria of Miller et al. (1981) suggest that both types are present. Chemical analyses were made of presumed primary white micas, which fall in the appropriate field of the Mg–Ti–Na diagram (Fig. 6) according to division established by Miller et al. (1981). They are also distinctively Fe-rich, similar to those in typical S-type granitoids of the Famatinian orogen (Table 2e) and those reported by Clarke et al. (2005) as coexisting with aluminous minerals. Thus, both textural and chemical evidence indicate a primary origin for some white micas of the Peñón Rosado granite.

3.3.6. Late felsic dykes

The magmatic association here is Pl–Qtz–Grt with Bt–Ms–Zrn-oxides as accessory minerals. Plagioclase is medium-grained, forms tabular sections, and is subhedral or occasionally anhedral, with Qtz–Bt-oxides as inclusions. Polysynthetic twinning and both normal and oscillatory optical zoning are observed, with occasional patchy zoning. Two plagioclases were analysed, one with continuous zoning (Pl_a, 3.9 × 2.7 mm), and one with oscillatory zoning (Pl_b, 1.3 × 0.7 mm). The Pl_a composition (average from two analyses) is $Ab_{70.8}$ $An_{27.9}$ $Or_{1.3}$ and the Pl_b reveals oscillatory zoning with a composition range between $Ab_{72.9}$ $An_{25.8}$ $Or_{1.3}$ and $Ab_{78.3}$ $An_{19.3}$ $Or_{2.3}$ (Table 2a). The garnet (1.9 × 1.7 mm) forms subhedral–euhedral hexagonal sections. The solid solution almandine–spessartine, constitutes 83.80 to 88.66% of the total molecular composition (Table 2c); pyrope, andradite and grossular make up the remainder. MnO content is high and the characteristic zoning pattern exhibits a relatively Mn-poor core and a relatively Mn-rich rim, constituting clearly a "spessartine inverse bell-shaped profile". Biotite and muscovite are sparse: the biotites are mantled by chlorite and the analysis

Table 2d
Representative compositions of dark micas in Peñón Rosado granite from electron microprobe analyses and structural formulae

Igneous unit	PRG				TG[a]	AG[b]
Igneous facies	PRG1	PRG2	PRG3	LFD	Average	Average
Sample/s	VCA-7079	ASP-114	ASP-111	ASP-112	TUA-246, 49	Plutonic rocks
Analysis number	Av. (n=4)	Av. (n=6)	Av. (n=8)	Av. (n=2)	Av. (n=6)	Av. (n=52)
Mineral	Bt[c]	Bt	Bt	Bt[d]	Bt	Bt
wt.%						
SiO_2	35.76±0.27	35.11±0.50	35.53±0.45	34.36±0.10	34.77±0.73	34.51±0.63
TiO_2	2.30±0.07	2.59±0.31	2.29±0.13	0.82±0.04	2.63±0.32	2.55±0.53
Al_2O_3	17.53±0.30	19.32±0.19	18.99±0.34	18.69±0.11	18.93±1.06	19.94±0.83
FeO	19.39±0.36	18.92±0.41	15.94±0.27	15.87±0.00	17.38±0.71	22.65±1.50
MnO	0.85±0.16	0.44±0.19	0.72±0.06	1.00±0.07	0.94±0.90	0.40±0.24
MgO	8.94±0.11	8.86±0.41	10.63±0.29	12.79±0.10	10.33±0.56	5.75±1.68
CaO	0.02±0.02	0.02±0.02	0.02±0.03	0.18±0.02	0.04±0.03	0.01±0.01
Na_2O	0.09±0.04	0.05±0.02	0.09±0.02	0.07±0.01	0.19±0.03	0.14±0.06
K_2O	9.65±0.19	9.74±0.10	10.30±0.50	6.16±0.12	8.90±0.59	9.40±0.22
F	0.32±0.16	0.11±0.07	0.50±0.05	0.09±0.02	0.17±0.03	1.17±0.46
Cl	0.01±0.00	0.02±0.01	0.04±0.01	0.01±0.01	bld	nd
Total	94.90±0.66	95.17±0.55	95.07±0.63	90.08±0.03	94.38±1.24	96.42±0.63
O_F_Cl	0.14±0.07	0.05±0.03	0.22±0.02	0.04±0.01	0.07±0.06	0.49
CTotal	94.76±0.61	95.12±0.54	94.85±0.62	90.04±0.02	94.31±1.26	95.93
Structural formulae calculated on basis 22 O						
Si	5.52	5.37	5.41	5.38	5.32±0.04	5.35
Al^{IV}	2.48	2.64	2.59	2.62	2.68±0.04	2.65
Sum-T	8.00	8.00	8.00	8.00	8.00±0.00	8.00
Al^{VI}	0.71	0.84	0.81	0.83	0.74±0.22	0.98
Ti	0.27	0.30	0.26	0.10	0.30±0.04	0.30
Fe^{2+}	2.50	2.42	2.03	2.08	2.23±0.11	2.92
Mn	0.11	0.06	0.09	0.13	0.12±0.13	0.05
Mg	2.06	2.02	2.41	2.99	2.36±0.12	1.33
Sum-B	5.65	5.64	5.60	6.13	5.74±0.07	5.58
Ca	0.00	0.00	0.00	0.03	0.01±0.00	0.00
Na	0.03	0.02	0.03	0.02	0.06±0.0	0.04
K	1.91	1.90	2.00	1.23	1.74±0.11	1.86
Sum-A	1.94	1.92	2.03	1.28	1.80±0.11	1.90
CF	0.31	0.11	0.48	0.09	0.16±0.13	1.15
CCl	0.00	0.01	0.02	0.00	0.00	0.00
$Fe^{2+}/(Fe^{2+}+Mg)$	0.55	0.55	0.46	0.41	0.49±0.02	0.69

References as in Table 2a for the plagioclases in PRG1. C=calculated. LFD=late felsic dyke. nd=not determined.
[a] Biotites in Tuaní Granite unit (cordierite-bearing granitoids), database from Dahlquist et al. (2005b).
[b] Biotites in andalusite-bearing granitoids, database from Clarke et al. (2005).
[c] Representative composition of biotite used in geothermobarometry and fractional crystallization model using major oxides, which result from the average of 4 samples (explanation in Section 7).
[d] Chloritized biotite.

reveals that the original composition has been partially modified (Table 2d). Quartz is abundant, rectangular to irregular and subhedral–anhedral.

3.4. Whole-rock geochemistry

3.4.1. Major elements

The Peñón Rosado granite has an average aluminium saturation index of 1.12 (Table 3) and is classified as a slightly peraluminous suite according to the nomenclature of Chappell and White (1992). It displays a distinct chemical trend compared with (a) the metaluminous granitoids of Cerro Asperecito (Fig. 2), (b) the typical Famatinian metaluminous granitoids of the Sierra de Chepes, (c) the Boggy Plain metaluminous supersuite, an extensive (500 km) and well-known belt of I-type granitoids in the central Lachlan Fold Belt of SE Australia, whose parental magma was derived by reworking of pre-existing crust in a similar way to that of the Famatinian granitoids (Wyborn et al., 1987; Pankhurst

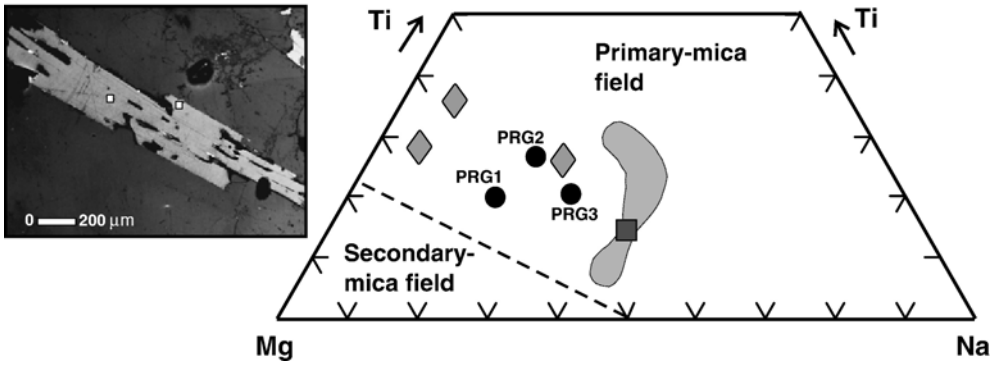

Fig. 6. Projected composition of white micas in the triangular diagram Mg–Ti–Na (data in Table 2e). The limit between fields for secondary and primary micas is from Miller et al. (1981). Grey field is representative of the white micas compositions in cordierite-bearing granitoids of Sierra de Chepes (Dahlquist et al., 2005b; data is showed in Table 2e). Filled rhombus are representative magmatic muscovite in garnet-bearing granitoids according to Kebede et al. (2001). Filled square is a typical value of Mg–Ti–Na from white micas (53 samples) crystallized in andalusite-bearing granites (Clarke et al., 2005; data is showed in Table 2e). Main inset shows representative primary white micas in PRG1 facies and the localization of two analyses (white squares). PRG: Peñón Rosado granite, facies 1, 2, and 3.

et al., 1998), and (d) a classical metaluminous suite defined in the original A–B diagram of Debon and Le Fort (1983) from a large database (Fig. 7a and b). The Peñón Rosado granite plots outside the main metaluminous trend and it is very difficult to envisage it as a differentiation product of metaluminous parent magma. The Peñón Rosado granite trend shown in Fig. 7b falls in the peraluminous domain of the diagram of Debon and Le Fort (1983). The transition from *m-p-g* (moderately peraluminous granitoids) to *f-p-g* (felsic peraluminous granitoids) strongly suggests a magmatic suite in which the extension of PRG3 into the *f-p-g* field represents a highly fractionated or residual peraluminous magma (see Villaseca et al., 1998). The Peñón Rosado granite trend is similar to those of the aluminous suites reported by Debon and Le Fort (1983).

The three main facies of the Peñón Rosado granite show a progressive increase in SiO_2 in the Harker variation diagrams (Fig. 8 and Table 3). PRG1 has higher CaO, Na_2O, Al_2O_3 and MnO concentrations, whereas PRG2 has higher FeO, MgO, TiO_2, P_2O_5 and K_2O, and PRG3 has the highest K_2O concentration. All major elements show a distinctive inflexion for the PRG2 facies (SiO_2=70.88%). The geochemical characteristics of the three facies are coherent with the magmatic mineral assemblage observed in each (e.g., PRG1 is plagioclase-rich, PRG2 is biotite-rich, and PRG3 is K-feldspar-rich).

3.4.2. Trace elements and REE

Harker plots for some trace elements (e.g., Th, Hf, Nb, Ta, Ga) also show an inflexion at SiO_2=70.88%, interpreted as signifying a change in the crystallization sequence. In addition, the similarity between the trace element inter-relationships (Ba, Sr and Rb) shown in Fig. 8 and those modelled by different authors (e.g., McCarthy and Robb, 1978; Rapela and Shaw, 1979) indicate that the main mechanism of differentiation was fractional crystallization in a closed system, without significant contamination of the magma during its evolution. PRG1 and PRG2 exhibit similar Zr concentrations, whereas PRG3 is depleted in Zr.

A distinctive chondrite-normalized REE pattern is exhibited by each PRG facies (Fig. 9 and Table 3). PRG1 has relatively low LREE and high HREE values ($[La/Yb]_N$=1.78), with marked positive Eu-anomalies (Eu/Eu*=1.95), strongly suggesting that it is probably accumulate. Conversely, PRG2 is characterized by relatively high LREE and low HREE values ($[La/Yb]_N$=8.31), with negative Eu-anomalies (Eu/Eu*=0.72). PRG3 is depleted in REE, with a flat pattern ($[La/Yb]_N$=3.64) and slightly negative Eu-anomalies (Eu/Eu*=0.82).

4. Geochronology

Zircons were separated from sample VCA-7079 (PRG1 facies) at NERC Isotope Geosciences Laboratory, U.K., and analysed for U–Pb isotopic composition using SHRIMP RG at The Australian National University, Canberra (as in Williams, 1998). The zircons are quite variable in morphology, with length: breadth ratios ranging from ~ 1 to ~ 3, the latter up to 250 µm long, and mostly subhedral. Cathodo-luminescence images (Fig. 10) show that the zircons are of crustal origin, with cores consisting of complex fragments of older grains (showing both sector-zoned and oscillatory zoned forms), overgrown by two stages of low-luminescence zircon thought to be related to crystallization of granite magma formed by anatexis. In order to define the

Table 2e
Representative compositions of white micas in Peñón Rosado granite from electron microprobe analyses and structural formulae

Igneous unit	PRG			TG[a]	AG[b]
Igneous facies	PRG1	PRG2	PRG3	TUA-246, 49	Plutonic rocks
Sample/s	VCA-7079	ASP-114	ASP-111		
Analysis number	Av. (n=4)	Av. (n=2)	Av. (n=5)	Av. (n=5)	Av. (n=53)
Mineral	WM[c]	WM	WM	WM	WM
wt.%					
SiO_2	45.39±0.24	44.28±0.07	44.85±0.88	45.39±0.39	45.43±0.55
TiO_2	0.68±0.02	0.65±0.02	0.71±0.06	0.84±0.33	0.55±0.53
Al_2O_3	32.01±0.42	33.96±0.00	33.22±0.26	33.23±0.41	35.21±1.44
FeO	4.23±0.08	3.22±0.05	3.47±0.13	3.49±0.16	1.83±0.68
MnO	0.03±0.02	0.01±0.01	0.03±0.02	0.03±0.03	0.03±0.03
MgO	1.03±0.09	0.62±0.01	0.83±0.05	0.75±0.05	0.85±0.41
CaO	0.04±0.02	bdl	0.01±0.01	bdl	0.01±0.02
Na_2O	0.34±0.07	0.24±0.01	0.42±0.04	0.60±0.05	0.65±0.18
K_2O	10.50±0.23	11.04±0.14	11.30±0.20	10.28±0.28	10.44±0.26
F	0.08±0.07	bdl	0.10±0.02	0.03±0.03	0.58±0.32
Cl	0.02±0.01	0.02±0.01	0.01±0.01	bdl	nd
Total	94.35±0.52	94.01±0.05	95.00±0.99	94.68±0.48	95.58±0.41
O_F_Cl	0.04±0.03	0.01±0.01	0.04±0.01	0.01±0.01	0.24
CTotal	94.31±0.52	94.01±0.05	94.95±0.99	94.67±0.49	95.24
Structural formulae calculated on basis 22 O					
Si	6.22	6.07	6.11	6.16±0.05	6.09
Al^{IV}	1.78	1.93	1.89	1.84±0.05	1.91
Sum-T	8.00	8.00	8.00	8.00±0.00	8.00
Al^{VI}	3.38	3.55	3.45	3.47±0.06	3.65
Ti	0.07	0.07	0.07	0.09±0.03	0.06
Fe^{2+}	0.49	0.37	0.40	0.40±0.18	0.21
Mn	0.00	0.00	0.00	0.00	0.00
Mg	0.21	0.13	0.17	0.15±0.01	0.17
Sum-B	4.15	4.12	4.09	4.11±0.04	4.09
Ca	0.01	0.00	0.00	0.00	0.00
Na	0.09	0.06	0.11	0.16±0.01	0.17
K	1.84	1.93	1.96	1.78±0.13	1.79
Sum-A	1.94	1.99	2.07	1.94±0.12	1.96
CF	0.07	0.00	0.08	0.03±0.03	0.49
CCl	0.01	0.01	0.01	0.00	0.00
$Fe^{2+}/(Fe^{2+}+Mg)$	0.70	0.75	0.70	0.72±0.02	0.55

References as in Table 2a for the plagioclases in PRG1. C=calculated. LFD=late felsic dyke. WM=white mica. nd=not determined.
[a] White micas in Tuaní Granite unit (cordierite-bearing granitoids), database from Dahlquist et al. (2005b).
[b] White micas in andalusite-bearing granitoids, database from Clarke et al. (2005).
[c] Representative composition of white mica (used in geothermobarometry and fractional crystallization model using major oxides, which result from the average of 4 samples (explanation in Section 7).

crystallization age of the granitoid, analysis spots were targeted in the non-luminescent rims. Eight such analyses were carried out (Table 4) and are plotted in a Tera–Wasserburg diagram (Fig. 10). Eliminating two results in which inheritance had clearly not been fully avoided, the remaining six data points give a well-defined crystallization age of 469±4 Ma (95% c.l. error, MSWD=0.7). This dates emplacement of the Peñón Rosado granite within the Mid-Ordovician according to Gradstein et al. (2004), and corresponds to Arenig–Llanvirn in traditional stratigraphical terms. This age is typical of Famatinian granitoids (Pankhurst et al., 1998, 2000).

5. Isotopic geochemistry

The Peñón Rosado granite has high initial range $^{87}Sr/^{86}Sr$ ratios from 0.70814 to 0.71093 and negative $\varepsilon(Nd)t$ values from −5.0 to −5.9 (Table 5). High Nd T_{DM} ages of 1.59 to 1.65 Ga (Table 5) were obtained using the multistage model of DePaolo et al. (1991). These isotopic data indicate that the parental magma was probably

Table 3
Representative major and trace element data of the Peñón Rosado granite and metaluminous granitoids in Cerro Asperecito

Igneous facies	Peñón Rosado granite						
	PRG1	PRG2			PRG3		
Sample	VCA-7079	ASP-108	ASP-114	ASP-216	ASP-215	ASP-217	ASP-214
Lithology	Garnet–Tdh	Garnet–Tn	Garnet–Tn	Garnet–Tn	Garnet–Mg	Garnet–Mg	Garnet–Mg
wt.%							
SiO_2	65.70	70.40	70.80	71.44	73.98	74.34	74.38
TiO_2	0.20	0.33	0.27	0.28	0.12	0.10	0.15
Al_2O_3	18.95	14.57	14.63	15.32	14.75	14.75	14.00
$Fe_2O_3^t$	2.71	3.41	2.99	3.21	1.44	1.42	1.90
MnO	0.44	0.10	0.10	0.14	0.09	0.08	0.08
MgO	0.84	1.10	0.91	0.93	0.40	0.33	0.48
CaO	4.11	3.66	3.18	3.66	2.03	1.59	2.42
Na_2O	5.32	3.12	3.46	3.40	3.50	3.34	3.45
K_2O	1.10	1.77	2.12	1.83	3.55	4.03	2.84
P_2O_5	0.05	0.15	0.11	0.14	0.08	0.09	0.08
LOI	0.63	0.55	0.40	0.39	0.39	0.61	0.86
Total	100.05	99.16	98.97	100.64	100.32	100.69	100.64
ppm							
Cs	3.30	2.82	1.88	2.20	2.10	1.60	2.20
Rb	49.00	73.48	81.89	66.00	86.00	97.00	78.00
Sr	248.00	214.00	200.90	202.00	152.00	105.00	148.00
Ba	107.00	360.87	392.35	316.00	601.00	391.00	447.00
La	17.40	36.65	38.19	20.90	13.00	12.30	17.60
Ce	36.80	74.56	77.83	43.40	27.50	26.90	36.80
Nd	11.00	29.44	30.17	4.76	3.00	2.95	4.09
Pr	3.19	7.77	8.08	17.80	11.00	11.60	15.30
Sm	1.98	5.63	6.05	3.59	2.45	2.73	3.43
Eu	1.10	1.17	1.21	0.95	0.79	0.63	0.80
Gd	1.52	4.48	5.23	3.36	2.42	2.74	3.47
Tb	0.40	0.67	0.90	0.58	0.43	0.54	0.65
Dy	3.83	3.34	5.04	3.71	2.68	3.29	3.88
Ho	1.10	0.63	1.06	0.84	0.56	0.65	0.78
Er	4.38	1.86	3.21	2.77	1.73	1.95	2.41
Tm	0.90	0.27	0.48	0.46	0.29	0.31	0.38
Yb	6.54	1.67	2.88	3.17	1.93	2.00	2.53
Lu	1.16	0.28	0.46	0.50	0.28	0.29	0.38
U	0.91	0.98	1.35	0.85	0.79	1.35	1.11
Th	4.60	11.12	12.51	7.17	4.72	4.82	6.40
Y	32.10	14.85	25.38	22.70	16.30	19.10	24.20
Nb	7.70	14.44	11.49	11.70	5.20	4.90	7.00
Zr	117.00	127.68	119.49	109.00	56.00	46.00	82.00
Hf	3.30	4.01	3.88	3.10	1.90	1.70	2.30
Ta	0.49	0.62	0.73	0.84	0.33	0.28	1.37
Ga	20.00	14.83	14.87	12.00	10.00	10.00	13.00
Ge	1.40	1.65	2.05	1.60	1.80	1.80	2.40
ASI	1.10	1.09	1.08	1.40	1.13	1.12	0.93

Igneous facies	Peñón Rosado granite			Metaluminous suites	
	PRG2		LFD		
Sample	ASP-111	ASP-218	ASP-112	Average[a]	ASP-119
Lithology	Garnet–Mg	Garnet–Mg	Garnet–FR	Tn/Gd	Mg
wt.%					
SiO_2	74.57	75.66	74.81	61.99±0.98	73.81
TiO_2	0.03	0.04	0.01	0.72±0.11	0.14

Table 3 (*continued*)

Igneous facies	Peñón Rosado granite			Metaluminous suites	
	PRG3		LFD		
Sample	ASP-111	ASP-218	ASP-112	Average[a]	ASP-119
Lithology	Garnet–Mg	Garnet–Mg	Garnet–FR	Tn/Gd	Mg
wt.%					
Al_2O_3	14.33	14.62	14.09	15.89±0.24	13.96
$Fe_2O_3^t$	0.81	0.78	0.72	7.07±0.48	1.60
MnO	0.09	0.05	0.22	0.13±0.01	0.04
MgO	0.14	0.12	0.07	2.67±0.13	0.32
CaO	1.09	1.12	2.51	5.05±0.41	0.92
Na_2O	3.38	3.39	4.53	2.50±0.28	2.91
K_2O	4.81	4.55	1.66	2.19±0.31	5.36
P_2O_5	0.09	0.09	0.07	0.21±0.04	0.21
LOI	0.59	0.48	0.29	0.98±0.14	0.65
Total	99.93	100.90	98.98	99.40±0.54	99.92
ppm					
Cs	1.79	5.00	0.80	4.65±1.13	8.68
Rb	149.17	123.00	40.60	98.92±17.7	243.21
Sr	52.64	64.00	126.13	182.00±13.2	54.49
Ba	170.16	217.00	207.29	360.29±73.4	226.29
La	3.83	5.24	8.24	27.78±2.69	26.45
Ce	8.05	11.40	14.06	59.47±4.45	56.25
Nd	3.12	1.27	4.52	22.29±1.30	22.35
Pr	0.83	5.73	1.32	5.80±0.30	5.99
Sm	0.99	1.48	1.00	4.61±0.58	5.52
Eu	0.36	0.40	0.62	1.10±0.16	0.67
Gd	1.18	1.64	0.96	3.84±0.94	4.85
Tb	0.27	0.34	0.24	0.66±0.19	0.9
Dy	1.94	2.27	1.85	3.98±0.85	5.00
Ho	0.39	0.44	0.48	0.79±0.20	0.90
Er	1.36	1.33	1.92	2.32±0.62	2.54
Tm	0.24	0.23	0.39	0.33±0.09	0.36
Yb	1.62	1.48	2.84	2.06±0.34	2.07
Lu	0.26	0.21	0.49	0.31±0.08	0.30
U	0.89	1.05	0.55	0.76±0.24	2.23
Th	0.94	1.95	1.49	6.68±1.45	12.32
Y	10.37	13.00	11.57	20.58±4.05	24.26
Nb	7.63	3.60	3.03	9.89±0.83	16.87
Zr	28.35	19.00	31.58	180.30±64.3	87.07
Hf	1.27	1.00	1.58	4.58±1.21	3.17
Ta	0.27	0.30	0.08	0.53±0.04	1.56
Ga	12.29	10.00	11.55	17.60±1.33	16.70
Ge	3.41	2.40	3.25	1.67±0.31	2.12
ASI	1.14	1.05	1.03	1.05	1.19

All major element oxides were analysed by ICP and trace element were analysed by ICP-MS in ACTLABS Canada. Total iron as Fe_2O_3; major element oxides in wt.%, trace element in ppm. Abbreviations: Tdh=trondhjemites; Tn=tonalites; Gd=granodiorites, Mg=monzogranites; FR: felsic rocks; PRG: Peñón Rosado granite; LFD=late felsic dykes; LOI=loss on ignition; bdl=below detection limit; nd=not determined. ASI=aluminium saturation index.

[a] Average from 5 samples. Samples from metaluminous suite in Cerro Asperecito are projected in Fig. 7a and b.

derived by partial melting of older lithosphere (middle crustal?), with negligible asthenospheric contribution.

6. Petrogenetic model

In order to define the main differentiation process during the crystallization, we have assessed two mathematical models as discussed below.

6.1. Fractional crystallization model based on major oxides

On the basis of the preceding observations (see Section 3.4.) it was assumed that the main mechanism of differentiation was fractional crystallization in a closed system, without significant contamination of the magma during its evolution. The fractionating mineral

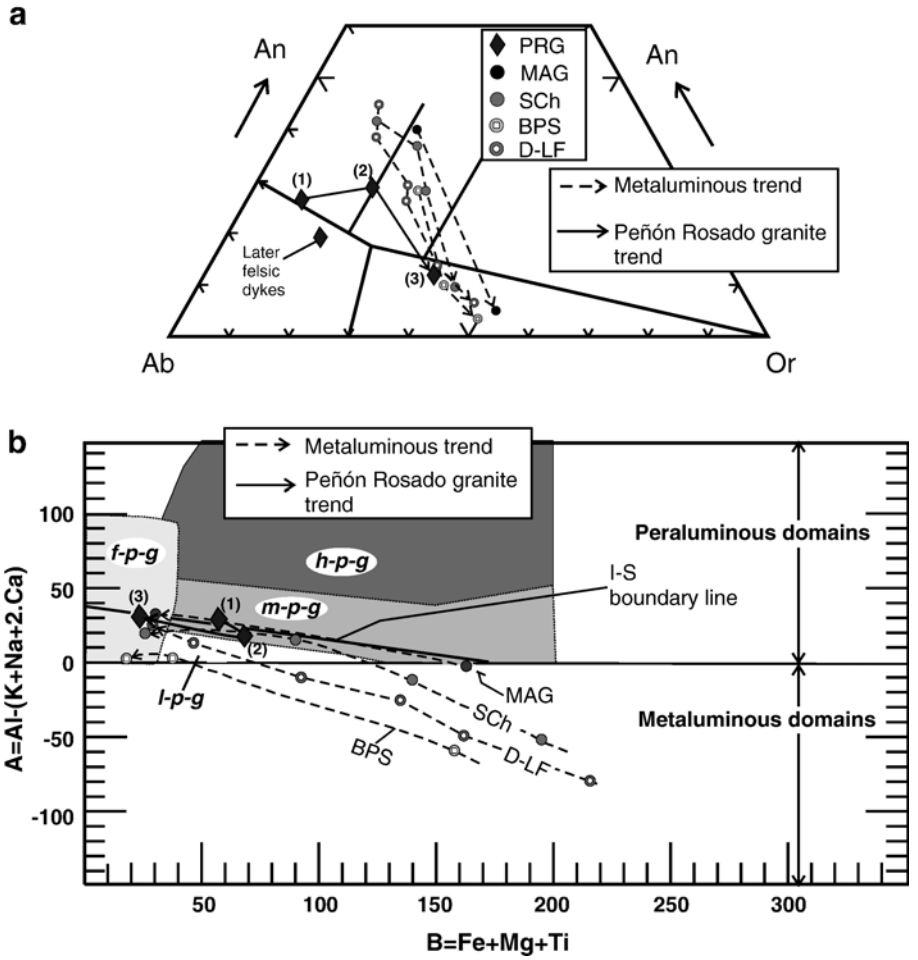

Fig. 7. (*a*) Granitoids plotted in terms of Ab–An–Or (Barker, 1979), showing different metaluminous trends and Peñón Rosado granite trend. (a) SCh=Sierra de Chepes metaluminous trend from Dahlquist et al. (2005a), including MME, Tn–Gd,GP, and Mz. MAG=metaluminous Asperecito granitoids, including Tn and Mz (data in Table 3); (b) BPS=Boggy Plain Metaluminous Supersuite, Lachlan Fold Belt, from Wyborn et al. (1987), including Gd, Ad, and Mz; (c) D-LF=Calc-alkaline metaluminous suites from the database of Debon and Le Fort (1983), including QD, MD, Tn, Gd, Ad, and Mz. The number next to each rhombus corresponds to the specific PRG facies in the Peñón Rosado granite. PRG1 (VCA-7079), SiO_2=65.70%; PRG2 (average 3 samples), SiO_2=70.88%; and PRG3 (average 5 samples), SiO_2=74.59%. QD=quartz diorite, MD=monzodiorite, MME=mafic microgranular enclaves, Tn=tonalites, Gd=granodiorites, GP=porphyritic granodiorites, Ad=adamellites, Mz=monzogranites. (*b*) A–B diagram after Debon and Le Fort (1983) and Villaseca et al. (1998), showing overall major element variation for the different metaluminous suites of (*a*). References in (*a*) I–S boundary line taken from Villaseca et al. (1998). Two different compositional domains are shown in the diagram, according to Debon and Le Fort (1983): with metaluminous area A<0 and peraluminous area A>0. Fields are: f-p-g (felsic peraluminous granitoids); h-p-g (highly peraluminous granitoids); m-p-g (moderately peraluminous granitoids); and l-p-g (low peraluminous granitoids).

assemblage in PRG1 is dominated by plagioclase (Table 1 and Fig. 8), with a significant change to produce the inflexion at ~ 71% SiO_2, coinciding with the switch to PRG2. Many authors have interpreted such abrupt inflections in element abundances as evidence for fractional crystallization as the principal process of magmatic differentiation (McCarthy and Robb, 1978; McCarthy and Groves, 1979; Rapela and Shaw, 1979; Chappell, 1997). Thus, during the crystallization of the PRG1 facies, large amounts of plagioclase were extracted yielding the increased concentration in this facies of, e.g., CaO, Na_2O, Al_2O_3, and Sr. Subsequently, voluminous biotite crystallization (together with apatite and monazite as distinctive accessory minerals) is verified in the PRG2 facies (Table 1), yielding the increase in FeO^t, MgO, TiO_2, and P_2O_5 (Fig. 8). As outcome of the fractionation of these elements in the PRG1 and

PRG2 facies, they are depleted in the SiO_2-rich rocks of PRG3 and the felsic late dykes (Fig. 8). The enrichment of K_2O and the trace element (Rb, Sr, Ba) inter-relationships shown in Fig. 8 for PRG3 indicate that abundant alkali feldspar appears in this facies after total crystallization of PRG2 (McCarthy and Robb, 1978; Rapela and Shaw, 1979).

Samples were chosen for use in fractional crystallization model taking into account textural relationships and both whole-rock and mineral chemistry. Thus, the VCA-7079 composition was assumed to represent the early crystallization of the PRG1 facies and the average composition of ASP-108, 114, and 216 was taken as the resultant evolved melt (PRG2); the parental magma from which PRG1 rocks accumulated to produce the differentiated PRG2 facies magma is considered as being composed of 30% of the former and 70% of the latter. A 30:70 mixture was chosen as representative of the parental magma because this yields the best fit in the fractional crystallization model (in the next section, this parental magma composition is also tested in a fractional crystallization model using REE). Least-square regression methods for modelling the segregation of crystallizing minerals (Bryan et al., 1969; Walker and Carr, 1986) were performed using IGPET program (Carr, 1998). Details of the calculations and the results are shown in Table 6 and Fig. 8. The fractional crystallization calculation shows a very acceptable ΣR^2 value (=sum of the squares of the residuals) for plutonic rocks (Dahlquist, 2002; Gomes and Neiva, 2005), and the calculated modal value of the early crystallized is similar to that of the sample analysed by electron microprobe (VCA-7079, PRG1 facies, Table 6). Nevertheless, the natural variables involved during magma crystallization in plutonic systems means that the numerical results of modelling (e.g., relative percentages of fractionating minerals) should be taken as no more than approximations to reality.

6.2. Fractional crystallization model based on trace elements

The same samples were also used for a trace element fractional crystallization model and geothermobarometry determinations (see Section 7). A quantitative trace element model was developed to compare the observed composition of the PRG2 with those obtained by calculation using the approach of Hanson (1978). The concentration of any trace element in the differentiated melt (C^L) relative to that in the parent melt (C_0) during fractional crystallization is given by the Rayleigh fractionation law:

$$C^{\mathrm{L}} = C_0 \cdot F^{(D-1)}$$

where F is the fraction of melt remaining and D is the bulk distribution coefficient of the fractionating assemblage, given by $D=\Sigma X_i \cdot K_i$, where X_i is the proportion of each mineral, and $K^{i/l}$ is its mineral–melt partition coefficient. $F=0.55$ as well as the initial concentration of REE elements were chosen from the results obtained in the previous section and both are shown in Table 7. K_i was assumed to be constant during the crystallization process; the values used and other details are founded in Table 7. There is a close correspondence between the observed and calculated values of C^{L} (differentiated melt) and C^{S} (cumulate), as is evident in Fig. 9.

Both fractional crystallization models using major oxides or trace element are consistent with PRG1 being a cumulate assemblage and PRG2 a differentiated melt, each derived from the hypothetical parental magma postulated here. Thus, the fractional crystallization was the main differentiation process in the Peñón Rosado granite.

7. Geothermometers and geobarometer applicable to Peñón Rosado granite

The texture and composition of garnet in the Peñón Rosado granite (Table 2c) are similar to those reported for typical magmatic garnet in granitic plutons (see Section 3.3 and discussion below). PRG1 biotites with high Mn contents (Table 2d) are typical of those crystallizing together with Mn-rich garnet (Leake, 1967; Miller and Stoddard, 1981). This suggests an equilibrium relationship between these two mineral phases, which were therefore used for geothermobarometric calculations. Anderson (1996) provided relevant recommendations for the use of the thermometer and barometer in igneous rocks and concluded that the Ganguly and Saxena (1984) geothermometer, using the Fe^{+2} and Mg partition between garnet and biotite, is the most robust version to account for the effects of high Mn, when CaO<10%. The R2 geobarometer model of Hoisch (1990) was used to calculate pressure, requiring the equilibrium crystallization of quartz, garnet, biotite, and plagioclase. The R3 model requires the crystallization of garnet, muscovite, quartz, and plagioclase minerals, whereas the R4 model requires crystallization of five mineral phases such as quartz, garnet, biotite, muscovite, and plagioclase. R3 and R4 yield unrealistic results, probably because the white mica compositional range of these models (Hoisch, 1990) does not correspond closely to that observed in the PRG1 facies.

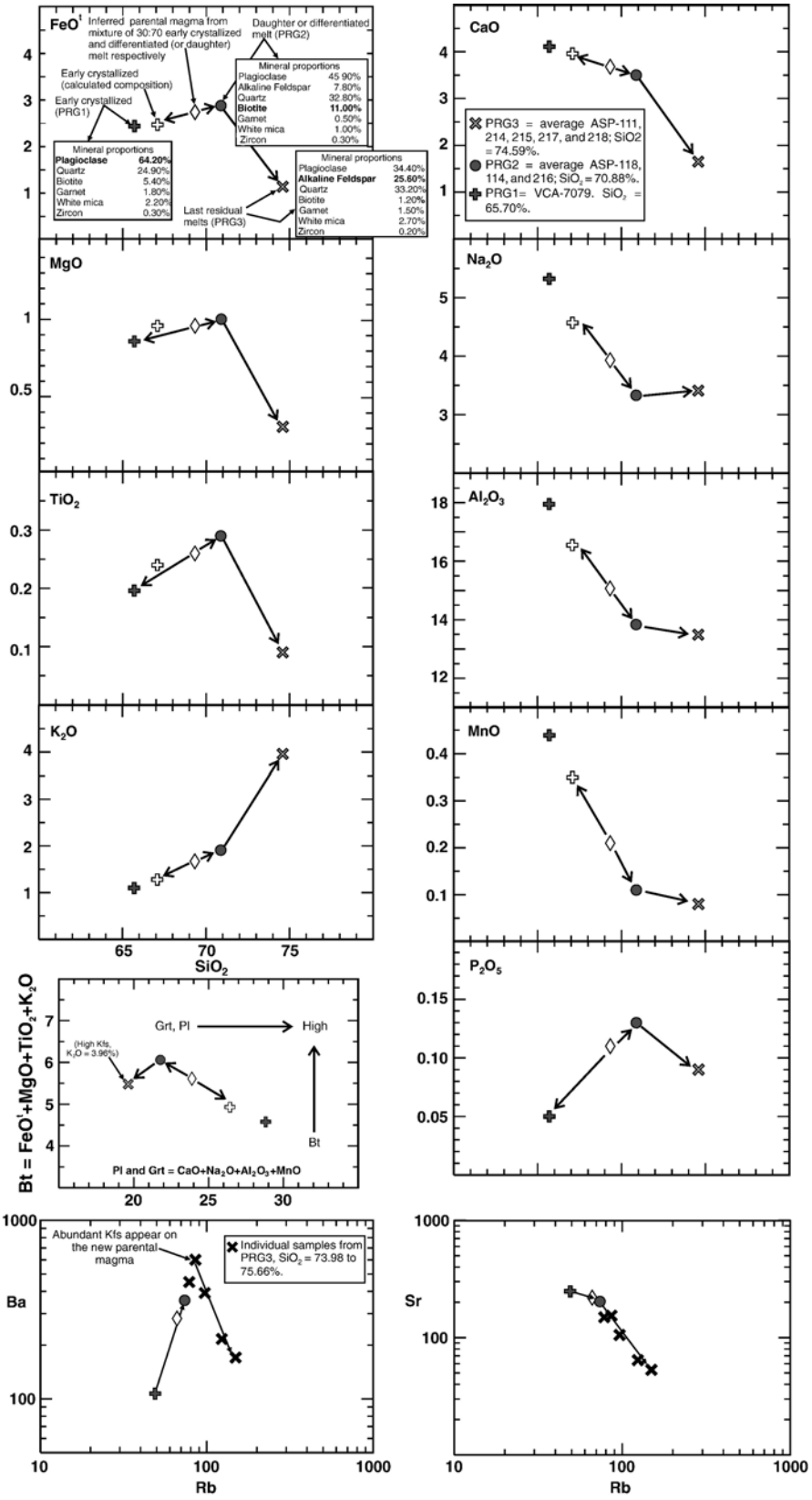
FeO*
Inferred parental magma from mixture of 30:70 early crystallized and differentiated (or daughter) melt respectively
Daughter or differentiated melt (PRG2)
Early crystallized (calculated composition)
Early crystallized (PRG1)
Mineral proportions
Plagioclase 64.20%
Quartz 24.90%
Biotite 5.40%
Garnet 1.80%
White mica 2.20%
Zircon 0.30%
Mineral proportions
Plagioclase 45.90%
Alkaline Feldspar 7.80%
Quartz 32.80%
Biotite 11.00%
Garnet 0.50%
White mica 1.00%
Zircon 0.30%
Mineral proportions
Plagioclase 34.40%
Alkaline Feldspar 25.60%
Quartz 33.20%
Biotite 1.20%
Garnet 1.50%
White mica 2.70%
Zircon 0.20%
Last residual melts (PRG3)
CaO
PRG3 = average ASP-111, 214, 215, 217, and 218; SiO2 = 74.59%.
PRG2 = average ASP-118, 114, and 216; SiO2 = 70.88%.
PRG1= VCA-7079. SiO2 = 65.70%.
MgO
Na2O
TiO2
Al2O3
K2O
MnO
P2O5
SiO2
Bt = FeO*+MgO+TiO2+K2O
Grt, Pl
High
(High Kfs, K2O = 3.96%)
Bt
Pl and Grt = CaO+Na2O+Al2O3+MnO
Abundant Kfs appear on the new parental magma
Individual samples from PRG3, SiO2 = 73.98 to 75.66%.
Ba
Sr
Rb
Rb

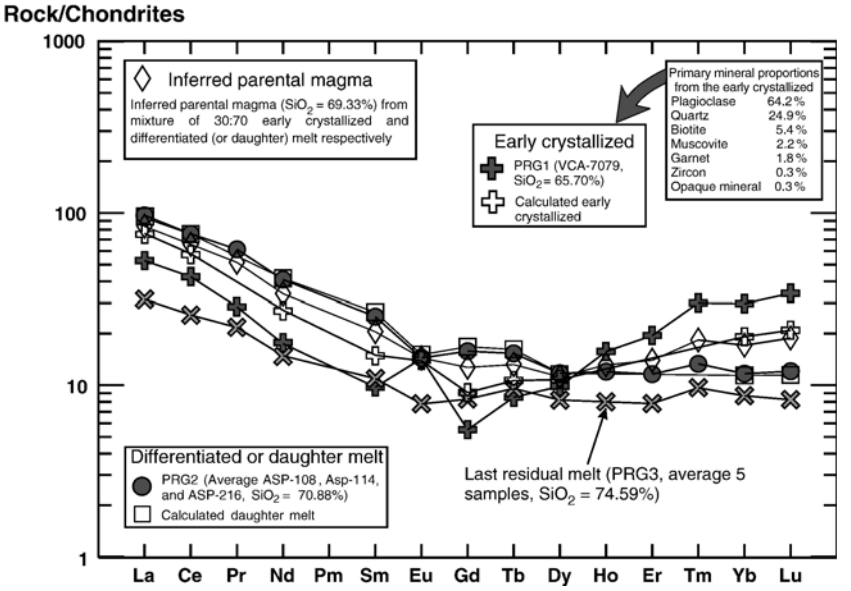

Fig. 9. Chondrite-normalized rare-earth element patterns for the Peñón Rosado granite. Results from the fractional crystallization model (empty rhombus, cross and circle) are shown in the figure and later explained in Section 6.2. The close agreement between observed and calculated patterns supports a fractional crystallization process. Chondrite concentrations according to Nakamura (1974). Tb, Ho, and Tm are according to Boynton (1984).

7.1. Calculated temperature and pressure

Compositional maps and zoning profiles of garnet in the PRG1 facies show three distinctive zones: a) central zone, b) intermediate compositional zone, and c) marginal rim zone, with a progressive increase in MnO (Fig. 5). The wide central zone was used to define the temperature of major garnet crystallization in this facies; an average of 7 representative analyses was used in combination with the average of 4 representative analyses from biotites (Table 8). The calibrations used here (Ganguly and Saxena, 1984; Hoisch, 1990) are functions of both pressure and the temperature. Therefore, they were solved by iteration, where the temperature obtained from the geothermometer was recalculated until it satisfied the pressure obtained from the geobarometer. The resultant temperature and pressure (T=784 °C and P=5.9 kb, Table 8) are consistent with crystallization of garnet and biotite under magmatic conditions. The generally accepted intersection of the granite solidus curve with experimental curves for the reaction

$$\mathrm{Ms} + \mathrm{Qtz} = \mathrm{Kfs} + \mathrm{Al} - \mathrm{silicates} + \mathrm{H_2O}$$

would suggest a depth of crystallization for muscovite in granitic magmas of at least 10–14 km (approximately 3–4 kb), and is consistent with the geobarometric result. In addition, estimated P and T using TWQ (Berman, 1991) and the activity–composition model for garnet (Berman, 1990) and biotite (McMullin et al., 1991) reveal very similar conditions (T=792 °C, P=6.0 kb; Table 8) to those obtained from the calibrations Ganguly and Saxena (1984) and Hoisch (1990). Finally, zircon saturation temperatures (T_{Zr}) calculated from bulk-rock compositions using the equation of Miller et al. (2003), yield a similar initial temperature of crystallization of 764 °C (Table 8). This T_{Zr} value is typical of granites rich in inherited zircon (average using 22 granitic samples = 766±24 °C, Miller et al., 2003). The results shown in Table 8 are reasonable for granitic bodies emplaced in a migmatitic high-grade terrane with a biotite–sillimanite association, indicating that the garnet and the sheet minerals have a certain magmatic origin.

8. Petrogenesis of the Peñón Rosado garnet pluton

8.1. Interpretation from petrography and mineral chemistry

Previous descriptions of Mn-rich garnets from felsic granitic rocks have recorded both types of zoning seen in

Fig. 8. Harker variation diagrams showing the main trend defined by the different facies and Ba, Sr, Rb inter-relationships for the Peñón Rosado granite. Results from the fractional crystallization model (rhombus and empty cross) are shown in this figure and later explained in Section 6.1. Rhombus and empty cross represent calculated parental magma and early crystallized respectively.

the Peñón Rosado granite (Section 3.3). Two main factors are operative in the formation of zoning: (a) the chemical potential (μ) value of the MnO component in the solid phase (garnet) relative to the chemical potential value of the MnO component in the melt phase, and (b) Mn diffusion within the crystal (Yardley, 1977; Manning, 1983; Spear, 1993). Taking the Gibbs free energy (see Ghiorso and Carmichael, 1987) for garnet saturation, we have for the crystallization reaction liquid → solid:

$$\Delta G = \mu_{\mathrm{MnO}}^{\mathrm{Garnet}} - \mu_{\mathrm{MnO}}^{\mathrm{Melt}} \quad (1)$$

so that if garnet is stable:

$$\mu_{\mathrm{MnO}}^{\mathrm{Garnet}} < \mu_{\mathrm{MnO}}^{\mathrm{Melt}} \quad (2)$$

(or $K_D > 1$, with Mn behaving as a trace element; e.g., Hollister, 1966; Atherton, 1968; Manning, 1983).

Because garnet crystallized throughout the crystallization sequence, expression (2) can be assumed as generally valid (our current understanding of the thermodynamics of silicate melts does not allow computation of the activity of Mn-bearing components in the melt, which vary as a function of P–T and the mole fraction for every phase). Therefore, diffusion is the main variable to be taken into account. As explained by different authors (e.g., Leake, 1967; Clarke, 1981; Manning, 1983) garnet zoning is an intrinsic feature of the growth mechanism and is controlled by the rate at which the necessary constituents (mainly Mn and Fe in our case) can diffuse to, and within, the growing crystal. As shown by various authors (e.g., Yardley, 1977; Spear, 1993), diffusion becomes exponentially more rapid with increasing temperature and diffusion rates for Mn in garnet are negligible below about 640±30 °C (Yardley, 1977; Manning, 1983; Harrison, 1988), but self-diffusion of the Mn cation in spessartine–almandine garnet above ~ 700 °C is sufficiently rapid to eliminate any compositional zoning during growth. Thus, the wide homogenous central zone (spessartine average = 28.96% for garnets in PRG1 and 23.11% in PRG2) implies crystallization at temperatures above ~ 700 °C, whereas the Mn enrichment in the marginal rims (spessartine average = 39.18% in PRG1 and 26.16% in PRG2) is due to retention and accumulation (negligible diffusion) of Mn during late crystallization at low temperatures (i.e., below ~ 700 °C, Fig. 5). The intermediate compositional zone of garnets in PRG1, with a spessartine range between 32.11 and 33.39%, may represent growth between ~ 700 and 600 °C with rapidly

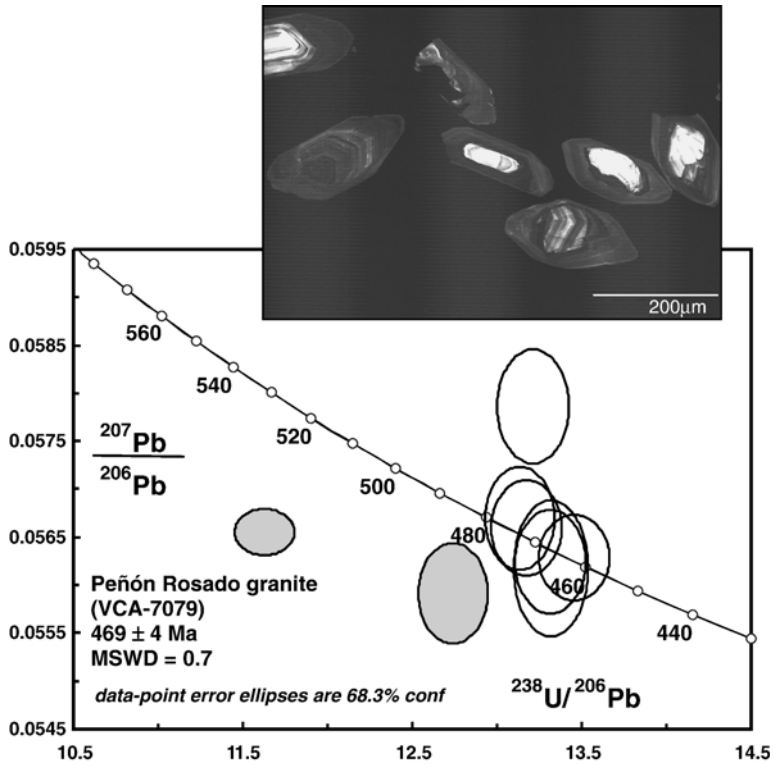

Fig. 10. Tera–Wasserburg diagrams for the Peñón Rosado granite (VCA-7079, PRG1 facies), error ellipses are 1; shaded points are excluded from the age calculation.

Table 4
Summary of SHRIMP U–Pb zircon results for sample VCA-7079

Grain. spot	U (ppm)	Th (ppm)	Th/U	$^{206}Pb^*$ (ppm)	$^{204}Pb/^{206}Pb$	f_{206} %	Total $^{238}U/^{206}Pb$	±	$^{207}Pb/^{206}Pb$	±	Radiogenic $^{206}Pb/^{238}U$	±	Age (Ma) $^{206}Pb/^{238}U$	±
1.1	863	42	0.05	56.3	0.000035	0.01	13.165	0.136	0.0566	0.0003	0.0759	0.0008	471.9	4.8
2.1	747	39	0.05	48.9	0.000031	0.02	13.127	0.137	0.0567	0.0004	0.0762	0.0008	473.2	4.8
3.1	650	20	0.03	42.3	0.000011	0.17	13.204	0.139	0.0579	0.0004	0.0756	0.0008	469.8	4.8
4.1	771	68	0.09	52.1	0.000029	<0.01	12.732	0.134	0.0559	0.0003	0.0786	0.0008	488.0	5.0
5.1	744	34	0.05	48.0	0.000022	<0.01	13.308	0.139	0.0562	0.0004	0.0752	0.0008	467.1	4.8
6.1	457	19	0.04	29.5	0.000096	<0.01	13.309	0.142	0.0562	0.0005	0.0752	0.0008	467.1	4.9
7.1	1007	48	0.05	64.3	0.000030	<0.01	13.449	0.139	0.0563	0.0003	0.0744	0.0008	462.3	4.7
8.1	5295	33	0.01	391.4	0.000006	<0.01	11.621	0.117	0.0566	0.0002	0.0862	0.0009	533.1	5.2

Notes:1. Uncertainties given at the one s level.
2. Error in FC1 reference zircon calibration was 0.16% for the analytical session (not included in above errors but required when comparing data from different mounts).
3. f_{206} % denotes the percentage of ^{206}Pb that is common Pb.
4. Correction for common Pb made using the measured $^{238}U/^{206}Pb$ and $^{207}Pb/^{206}Pb$ ratios following Tera and Wasserburg (1972) as outlined in Williams (1998).

decreasing Mn diffusion. Similarly, the unzoned garnets in PRG3 involve crystallization at temperatures above ~ 700 °C and high Mn diffusion, and the absence of Mn enrichment in the rims suggests that crystallization ceased above ~ 700 °C. Thus the zoning profile of garnet in PRG1, as well as the geothermobarometric calculations (Table 8), indicate major garnet crystallization from a granitic magma at middle pressures (6 kb) and moderate–low magmatic temperatures (764–792 °C) (Figs. 5 and 11). Remarkably, this is the main reason for which a "spessartine inverse bell-shaped profile" or unzoned is expected for magmatic garnets crystallizing above ~ 700 °C, and "spessartine bell-shaped profile" for Mn-rich garnets growing under low-grade metamorphic conditions or crystallizing below ~ 700 °C in very felsic magmas (i.e., SiO_2=73–76%; Leake, 1967; Miller and Stoddard, 1981; Manning, 1983).

In the KFMASH system, a classic reaction proposed for the anatectic generation of peraluminous partial melt from metagreywackes (Vielzeuf and Holloway, 1988) (Fig. 11) is

$$Pl + Bt + Sil + Qtz = Grt_{MET}/Crd_{MET} + Kfs + melt \quad (3)$$

The lack of metamorphic garnet and cordierite in the exposed migmatitic gneiss of Cerro Asperecito (in which the Peñón Rosado granite was emplaced) suggests that the parental magma was derived from unexposed metamorphic basement.

Table 5
Rb–Sr and Sm–Nd data for different facies in Peñón Rosado granite

	SiO_2(wt.%)	Age (Ma)	Rb	Sr	$^{86}Rb/^{87}Sr$	$(^{87}Sr/^{86}Sr)_{today}$	$(^{87}Sr/^{86}Sr)t$	εSr(*t*)
Peñón Rosado granite (t=469 Ma)								
PRG1 (VCA-7079)	65.70	469	49	248	0.5720	0.714749	0.710926	99.12
PRG2 (ASP-108)	70.40	469	73	214	0.9877	0.715628	0.709027	72.15
PRG2 (ASP-114)	70.80	469	82	200	1.1872	0.716072	0.708138	59.52
LFD (ASP-112)	74.57	469	41	126	0.9423	0.716429	0.710132	87.84

	SiO_2 (wt.%)	Age (Ma)	Sm	Nd	$^{147}Sm/^{144}Nd$	$(^{143}Nd/^{144}Nd)_{today}$	$(^{143}Nd/^{144}Nd)t$	εNd(*t*)	T_{DM} *(Ga)
Peñón Rosado granite (t=469 Ma)									
PRG1 (VCA-7079)	65.70	469	2.0	11.0	0.1088	0.512068	0.511733	−5.9	1.65
PRG2 (ASP-108)	70.40	469	5.6	29.4	0.1158	0.512104	0.511747	−5.6	1.63
PRG2 (ASP-114)	70.80	469	6.1	30.2	0.1211	0.512148	0.511776	−5.0	1.59
LFD (ASP-112)	74.57	469	1.0	4.5	0.1337	0.512169	0.511758	−5.4	1.62

The decay constants used in the calculations are the values $\lambda^{87}Rb = 1.42 \times 10^{-11}$ and $\lambda^{147}Sm = 6.54 \times 10^{-12}$ $year^{-1}$ recommended by the IUGS Subcommision for Geochronology (Steiger and Jäger, 1977). Epsilon-Sr (εSr) values were calculated relative to a uniform reservoir present day: $(^{86}Rb/^{87}Sr)^{today}{}_{UR}$=0.0827; $(^{87}Sr/^{86}Sr)^{today}{}_{UR}$=0.7045. Epsilon-Nd (εNd) values were calculated relative to a chondrite present day: $(^{143}Nd/^{144}Nd)^{today}{}_{CHUR}$=0.512638; $(^{143}Sm/^{144}Nd)^{today}{}_{CHUR}$=0.1967.
t=time used for the calculation of the isotopic initial ratios. T_{DM}*=calculated according to DePaolo et al. (1991). PRG=Peñón Rosado granite. The numbers indicating facies 1 and 2. LFD=late felsic dykes.

Table 6
Results of fractional crystallization model for the Peñón Rosado granite

Calculated weight fractions (%) in the parental magma	Calculated extracted phases in the early crystallized (modal %)	Minerals utilized in the calculation (VCA-7079)[a]	Modal values from VCA-7079[b]
26.10	58.70	Plagioclase	Plagioclase.....64.20%
12.20	27.50	Quartz	Quartz.....24.90%
4.20	9.50	Biotite	Biotite.....5.40%
1.10	2.30	Muscovite	White mica.....2.20%
0.80	2.00	Garnet	Garnet.....1.80%

	SiO_2	TiO_2	Al_2O_3	FeO^{total}	MnO	MgO	CaO	Na_2O	K_2O	P_2O_5
Weight fractions (%) of magma remaining with a composition equal to PRG2 (daughter magma) = 55.3										
Parental magma[c]	69.33	0.26	16.07	2.74	0.21	0.94	3.68	3.93	1.67	0.11
Determined parental magma	70.07	0.26	16.24	2.77	0.21	0.95	3.72	3.97	1.69	0.11
Calculated parental magma	70.07	0.27	16.25	2.76	0.22	0.99	3.74	3.93	1.67	0.07
	0.00	−0.01	−0.01	0.02	−0.01	−0.04	−0.02	0.05	0.02	0.05
$\Sigma R^2 = 0.007$										
Early crystallized (VCA-7079)	65.70	0.20	18.95	2.44	0.44	0.84	4.11	5.32	1.10	0.05
Early crystallized (calculated)[d]	67.03	0.24	17.52	2.48	0.33	0.91	3.97	4.60	1.32	nd

Determined and *calculated* parental magma compositions were obtained using IGPET program (Carr, 1998). This program makes fractional crystallization calculations using least-squares regression of the major elements, after Bryan et al. (1969).
ΣR^2 = sum of the squares of the residuals.
[a] Mineral chemistry in Table 2. The samples are: plagioclase average with $n=4$, garnet average with $n=7$, biotite average with $n=4$, white mica average with $n=5$ and quartz (one analyses): $SiO_2=98.26\%$, $FeO=0.03\%$, $Na_2O=0.01\%$, $K_2O=0.03\%$.
[b] Modal proportions in Table 1.
[c] *Daughter magma* is the resulted of the average between ASP-108, ASP-114, and ASP-216 (PRG2); *parental magma* is derived from simple mixing of early crystallized (30% VCA-7079, PRG1) and daughter magma (70%, PRG2), and *early crystallized* is represented by VCA-7079. All data in Table 3.
[d] Σ(proportion modal × mineral chemistry used in the calculation).

The petrological and geochemical evidence indicates that the appearance of garnet in Peñón Rosado granite result of the direct nucleation and subsequent crystallization from the peraluminous magma, as indicated by other authors for garnet crystallizad in felsic granites (e.g., Clarke, 1981; du Bray, 1988; Harrison, 1988; Kebede et al., 2001). Therefore, the reaction most probable for garnet crystallization is (Fig. 11)

$$\text{Magma} \rightarrow \text{Grt}_{MAG} + \quad \text{Other Solid Phases.} \qquad (4)$$

The compositional data and the physical conditions of crystallization reported in this work for solid phases such as biotite or white mica (see also below) are consistent with magmatic equilibration with garnet.

The whole-rock geochemistry (Table 3) shows that the MnO/(FeO+MnO+MgO) ratios decrease from PRG1 (VCA-7079=0.12%) to PRG2 (ASP-114=0.03%), but increase again during the crystallization of PRG3 (ASP-111=0.1%), reaching their highest values in the late felsic dykes (ASP-112=0.23%). Sympathetically, PRG garnets have the following Mn/(Fe+Mn+Mg) ratios (Table 2c): VCA-7079=0.37, ASP-114=0.25, ASP-111=0.40; and ASP-112=0.38. Thus fractionation of Mn in garnet as well as the proportion of garnet that crystallizes (Table 1) is roughly controlled by the evolving composition of the different granitic facies.

The consistently high Al^{IV} in the biotites of all facies of the Peñón Rosado granite strongly suggests that their alumina contents were buffered by equilibration with an Al-rich phase, probably under constant temperature and pressure conditions, and the presence of garnet and primary white mica is consistent with a relatively Al_2O_3-enriched magma. Dahlquist et al. (2005b) and Clarke et al. (2005) report comparable Al^{IV} contents in biotites for other peraluminous rocks with magmatic cordierite or andalusite (Table 2d). The biotites have high $Fe^{2+}/(Fe^{2+}+Mg)$ ratios, except for those in the more differentiated facies such as PRG3, suggesting that the Fe was consumed during earlier crystallization. Remarkably, the early-crystallized PRG1 biotites have higher MnO contents (0.72 to 1.12%, Table 2d). Miller and Stoddard (1981) affirm that biotites coexisting with garnets have higher MnO>0.75%, than the 0.2 to 0.5% typical of igneous biotites without coexisting garnet. The lower MnO content for PRG2 and PRG3 biotites results from scavenging of MnO by the biotites and garnets crystallizing in PRG1.

Table 7
Data used in the fractional crystallization mathematical model for the Peñón Rosado granite

Minerals	Modal proportion (VCA-7079)	$K_d^{S/L}$ (La)	$K_d^{S/L}$ (Ce)	$K_d^{S/L}$ (Nd)	$K_d^{S/L}$ (Sm)	$K_d^{S/L}$ (Eu)	$K_d^{S/L}$ (Gd)	$K_d^{S/L}$ (Tb)	$K_d^{S/L}$ (Dy)	$K_d^{S/L}$ (Yb)	$K_d^{S/L}$ (Lu)
Pl	0.642	0.30^{+}	0.35^{-}	0.29$^{\#}$	0.34^{-}	1.11$^{@}$	0.13$^{\#}$	0.14^{+}	0.13^{+}	0.08*	0.06*
Qtz*	0.249	0.02	0.01	0.02	0.01	0.06	0.02	0.02	0.02	0.02	0.01
Bt^{+}	0.054	7.93	5.93	3.30	2.65	2.65	2.52	2.39	2.08	1.80	2.00
Ms^	0.022	6.04	7.11	10.81	6.72	1.89	4.19	5.50	2.97	7.25	7.74
Grt*	0.018	0.39	0.70	0.60	2.70	0.52	10.50	11.90	28.60	43.48	39.78
Zrn*	0.003	16.90	16.75	13.30	14.40	16.0	12.00	37.00	47.40	191.00	264.50
		La	Ce	Nd	Sm	Eu	Gd	Tb	Dy	Yb	Lu
C_o		31.44	64.38	24.16	4.68	1.16	3.86	0.67	3.95	3.56	0.61
Results obtained from the fractional crystallization mathematical model C_L^i (concentration in ppm)											
		La	Ce	Nd	Sm	Eu	Gd	Tb	Dy	Yb	Lu
WR_L^i REE		31.93	65.27	25.80	5.09	1.11	4.36	0.72	4.03	2.57	0.41
Calculated liquid C_L^i REE		31.73	65.18	26.22	5.40	1.16	4.62	0.76	4.03	2.53	0.39
WR_S^i REE		17.40	36.80	11.00	1.98	1.10	152	0.40	3.83	6.54	1.16
Calculated solid C_S^i REE		25.07	50.04	17.22	3.04	1.07	2.5	0.5	3.70	4.21	0.71

Equation describing fractional crystallization is the equation for Rayleigh fractionation: $C_L^i = C_0 \cdot F^{(D-1)}$.
C_0: the weight concentration in the parental melt is a mixing from 30% PRG1 cumulate (VCA-7079) and 70% of fractionated melt PRG2 (ASP-108, ASP-114, and ASP-216 average). Data in Table 3.
D=bulk distribution coefficient of the fractionating assemblage during crystal fractionation=$\Sigma X \times K_d^{S/L}$, where X is the mineral proportion crystallizing from the parental magma, and $K_d^{S/L}$ is the solid–liquid partition coefficient of phase i. X=modal proportions of VCA-7079 (Table 1).
F=weight fraction of melt produced in fractional crystallization. F is 0.55.
$WR_L i$=whole-rock liquid is the average composition of the PRG2 facies. Data in Table 3.
C_L^i=weight concentration of a trace element "i" in the fractionated melt.
$WR_S i$=whole-rock solid is the composition of VCA-7079 (PRG1 facies). Data in Table 3.
C_S^i=weight concentration of a trace element "i" in cumulate crystallized.
The partition coefficient for granitic liquids: data from *Rollinson (1993, Table 4.1), $^{+}$Nash and Crecraft (1985), ^du Bray (1994),–Nagasawa and Schnetzler (1971), $^{@}$Fujimaki et al. (1984), and $^{\#}$Arth (1976).

The petrographic and compositional characteristics of some of the Fe-rich white micas in the Peñón Rosado granite (Fig. 6) indicate a magmatic origin (Miller et al., 1981; Clarke et al., 2005; Dahlquist et al., 2005b) and are therefore indicative of a parental peraluminous magma.

The patchy zoning of PRG1 plagioclases is interpreted as due to resorption of early growth and infilling of the corroded regions by more sodic material (Vance, 1962; Anderson, 1984). This is consistent (together with the field evidence and textural characteristics of the microcline described in Sections 3.2 and 3.3 respectively) with the assumption that PRG1 is an older, plagioclase-rich facies, segregated early from the parental magma and reheated during intrusion of the later facies. The oscillatory compositional zoning of plagioclase in PRG3 and late felsic dykes may indicate final shallow crystallization with cyclic changes in temperature and pressure accompanying convective overturn. Alkali feldspar is only conspicuously present in PRG3, strongly suggesting that this facies is a residual melt saturated in K_2O, whereas its absence in late felsic dykes suggests that K_2O was mostly consumed during the earlier PRG3 crystallization.

8.2. Interpretation from whole-rock geochemical data

Major element geochemical data indicate that the PRG2 facies represents a differentiated melt from a parental magma due to removal of material in PRG1. The latter facies has higher Al_2O_3, CaO, Na_2O, MnO and lower FeO^t, MgO, TiO_2, P_2O_5 contents, consistent with plagioclase accumulation and crystallization of garnet with minor biotite–muscovite and apatite. PRG2 has higher FeO^t, MgO, TiO_2, K_2O, and P_2O_5 consistent with crystallization of biotite along with muscovite, apatite, and felsic minerals. This facies represents a compositional inflexion between PRG1 and PRG3, strongly suggesting the onset of crystallization of a new assemblage mineral. The fractional crystallization model supports a parental magma represented by a mixture 30% PRG1 and 70% PRG2, where PRG1 and PRG2 are early crystallized and differentiated melt respectively. PRG3 represents a late residual melt after total crystallization of the PRG2 facies, and is depleted in major oxides except for MnO and K_2O. Sample ASP-112 is a late felsic dyke with plagioclase and garnet; the absence of alkali feldspar indicates that the K_2O was consumed in PRG3.

Table 8
Geothermobarometry for Peñón Rosado granite

Peñón Rosado granite, PRG1 facies, sample VCA-7079			
Calibration	Mineral assemblage/Zr concentration (ppm)	Geothermobarometry	
		Temperature (°C)	Pressure (kbar)
Ganguly and Saxena (1984)	Garnet–biotite	784[a]	
Hoisch (1990) R2 model	Garnet–biotite–plagioclase–quartz		5.9±0.1
TWQ Berman (1991)[b]	Garnet–biotite	792	6.0
Zircon saturation temperature (T_{Zr})[c]	117[d]	764	

T–P calculated by interaction. Temperature values calculated according to the calibrations of Ganguly and Saxena (1984) are calculated until it satisfies the pressure obtained according to the calibration of Hoisch (1990).
Garnet composition from the average of 7 analysis: $n=7$, central zone of Grt_a (Table 2c).
Biotite composition from the average of 4 analysis: $n=4$, Table 2d.
White mica composition from the average of 4 analysis: $n=4$, Table 2e.
Plagioclase composition from the average of 4 analysis: $n=4$, Table 2a.
[a] See uncertainty discussion in Ganguly and Saxena (1984) and Anderson (1996).
[b] Activity–composition model for garnet from Berman (1990) and biotite from McMullin et al. (1991).
[c] $T_{Zr}=12{,}900/[2.95+0.85\,M+\ln(476{,}000/Zr_{melt})]$, where $D^{Zr,zircon/melt}=(476{,}000/Zr_{melt})$, is the ratio of Zr concentrations (ppm) in zircon to that in the saturated melt; M is a compositional factor that accounts for dependence of zircon solubility on SiO_2 and peraluminosity of the melt [(Na+K+2·Ca)/Al·Si), all in cation fraction]. Equation and Zr concentrations (ppm) in zircon (=476,000 ppm) from Miller et al. (2003).
[d] Zirconium concentration from VCA-7079 (PRG1 facies), Table 3.

Trace element concentrations in the different facies are coherent with the interpretations obtained from the major oxides. Thus, the change from low Ba in PRG1 to higher Ba in PRG2 (Fig. 8) indicates the onset of biotite and muscovite crystallization, whereas the distinct compositional change between PRG2 and PRG3 supports a new fractionation trends resulting in abundant alkali feldspar crystallization (McCarthy and Robb, 1978; Rapela and Shaw, 1979), where ASP-215 (Ba=601 ppm) is the first and ASP-111 (Ba=170 ppm) is the last crystallized. Rb, a typical incompatible element concentrated in residual melts, reaches its highest concentration in PRG3. The high Sr content in PRG1 is coherent with the accumulation of plagioclase in this facies, and Sr contents decrease with differentiation from PRG1 to PRG3. Zr content varies little between PRG1 and PRG2, but

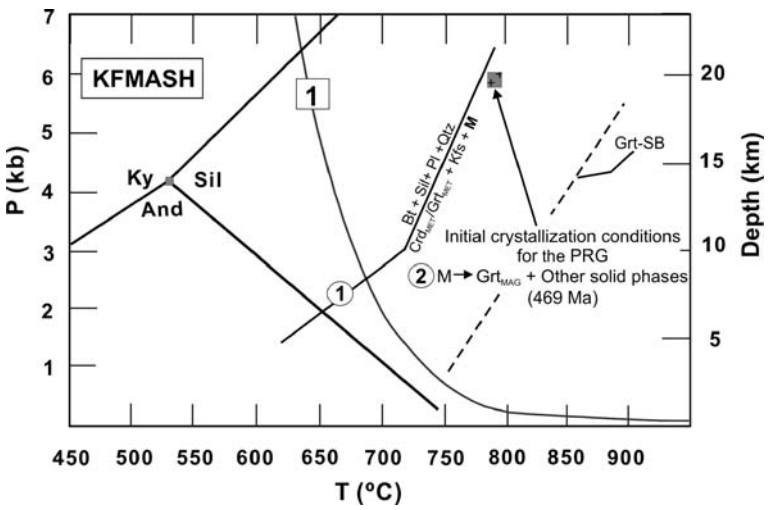

Fig. 11. Simplified *P–T* grid showing conditions of metamorphism and melt generation for the Peñón Rosado granite together with selected univariant reactions. Reaction 1 in the KFMASH system from Pattison and Tracy (1991) and Vernon et al. (2001). Grt-SB: stability boundary for garnet according to Clemens and Wall (1981). Al_2SiO_5 phase relations according to Guowei et al. (1994). Triple point (530 °C±20 °C and 4.2 kb±0.3 kb) according to Bohlen et al. (1991). Square '1', haplogranitic water-saturated solidus. Reaction 2 for garnet crystallization is discussed in the text. Bt=biotite, Sil=sillimanite, Qtz=quartz, Crd=cordierite, Grt=garnet, Kfs=alkali feldspar, And=andalusite, Ky=kyanite, M=melt, MAG=magmatic, MET=metamorphic.

decreases abruptly between PRG2 and PRG3, suggesting little crystallization of zircon in the residual melt.

Sawyer (1987), using mathematical modelling, suggested that REE patterns in different layers of migmatites may help to distinguish whether leucosomes represent pure melts or segregated cumulates. In addition, Johannes et al. (2003) have investigated metasedimentary migmatite and related small-scale S-type granites and conclude that the chemical signature (e.g., REE patterns) can distinguish between felsic cumulates (represented by leucosome in migmatite) and differentiated or primary melts (represented by S-type granites). The PRG2 facies has relatively high REE contents and negative Eu-anomalies (Fig. 12), similar to rocks interpreted as melt derived from migmatites, whereas PRG1 has relatively low REE and positive Eu-anomalies, as in the corresponding cumulate material (Sawyer, 1987; Johannes et al., 2003). Thus, chemical signature and the fractional crystallization model (using REE and major oxides) are fully consistent with a fractional crystallization process where PRG1 represent a felsic cumulate and PRG2 a differentiated melt.

Geochemical characteristics and isotopic ratios (Table 5) are consistent with derivation of the Peñón Rosado granite by partial melting of the metasedimentary rocks. Sylvester (1998) argued that the CaO/Na_2O ratios in S-type peraluminous granitoids are controlled by the original proportion of plagioclase in the source rock. Thus, S-type peraluminous melts produced from clay-rich sources (plagioclase-poor) tend to have lower CaO/Na_2O ratios (<0.3) than melts derived from sources which are clay-poor (plagioclase-rich, CaO/Na_2O ratios >0.3). The CaO/Na_2O of 1.04 for the assumed parental melt of the Peñón Rosado granite (Table 6), together with the discrimination diagram of Sylvester (1998), indicates a clay-poor source such as metagreywacke (Fig. 13).

The CaO% content of the inferred parental melt is remarkably high (3.68%, Table 6). Experimental dehydration melting of metagreywacke (Patiño Douce and Beard, 1996) produced melts with $CaO=0.73\%$ to 1.67%. However, because increasing H_2O activity depresses the plagioclase+quartz solidus more strongly than it depresses the stability of micas (Patiño Douce, 1996; Patiño Douce and Harris, 1998), H_2O-fluxed melting consumes plagioclase more effectively than micas, increasing the CaO and the Na_2O in the melt. In agreement with this, Holtz and Johannes (1991) determined that with increasing amounts of H_2O the melt becomes richer in CaO, FeO and Na_2O and poorer in K_2O, and that CaO/Na_2O ratios increase progressively. These experimental data explain the high CaO/Na_2O ratios and low K_2O content in the hypothetical parental magma. Among dehydration reactions (e.g., Vielzeuf and Holloway, 1988; Patiño Douce and Harris, 1998) only muscovite may undergo substantial dehydration at $T<800$ °C (Miller et al., 2003), and in consequence

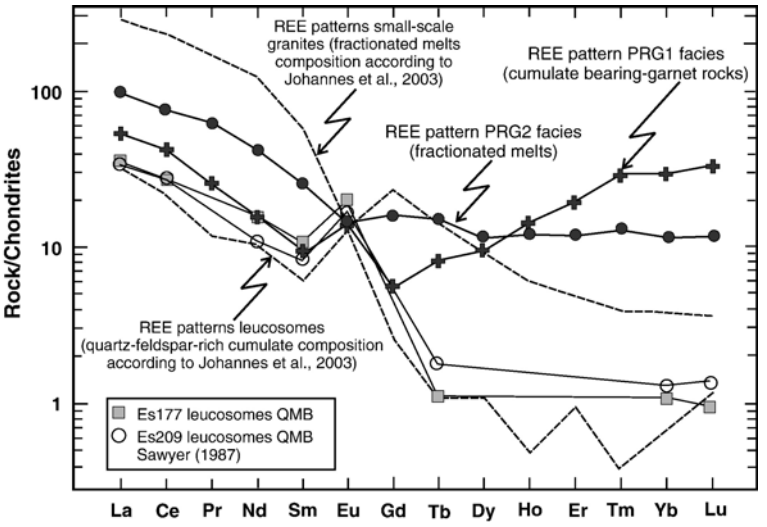

Fig. 12. Modified from Johannes et al. (2003, Fig. 12). Upper broken line is the REE pattern for small-scale granites from Turku, Finland, interpreted as fractionated from a primary undifferentiated melt derived by partial melting of metasedimentary migmatites during the metamorphic peak (830 °C and 6 kbar; cordierite, garnet and partial melt are the most important reaction products). Lower broken line is the REE pattern of leucosomes in migmatites from Turku, which are interpreted as cumulates segregated from the primary melt. The low normalized Tm and Ho values are due to analytical uncertainties (Johannes et al., 2003). Other REE patterns of the migmatite leucosomes interpreted as cumulates are from Sawyer (1987). Solid line and full black circles and crosses define the REE pattern for the PRG1 and PRG2 facies.

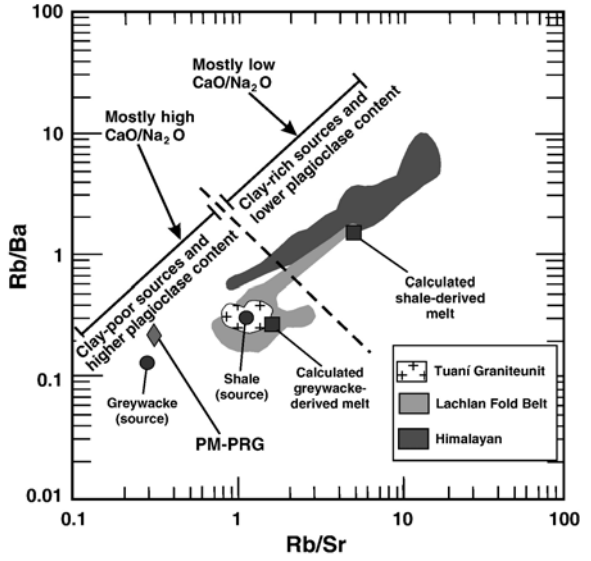

Fig. 13. Rb/Sr vs. Rb/Ba diagram for strongly peraluminous granitoids modified from Sylvester (1998). The dark fields, discontinuous line, and calculated melt are from Fig. 7 of Sylvester (1998). Geochemical data of the Tuaní Granite unit (cordierite-bearing granitoids) in the Sierra de Chepes from Dahlquist et al. (2005b). PM-PRG=composition of the assumed parental magma for the Peñón Rosado granite.

muscovite must be abundant (e.g., pelitic source) for this to result in anatexis. However, the composition of the parental magma of Peñon Rosado granite is not consistent with a pelitic source, and it is more probably a result of H_2O-fluxed melting of metagreywacke. The crystallization of the Peñón Rosado granite (469 Ma) was almost synchronous with that of a major metaluminous suite emplaced during the Middle Ordovician (468 Ma; Pankhurst et al., 2000) in similar P–T conditions (Dahlquist et al., 2006), suggesting that the latter may have been the cause of anatexis of the surrounding metasediments. The small exposed area of the Peñón Rosado granite (only ~ 5% at Cerro Asperecito) relative to the metaluminous granitoids outcrops in this region implies that heat input from a major batholith was required in order to generate a small amount of peraluminous magma.

9. Conclusions

All available data, including field and petrographic relationships, mineral chemistry, bulk major and trace element compositions, and isotopic ratios support differentiation by fractional crystallization in the middle crust, including the crystallization of magmatic garnet. The crystallization sequence has three main stages represented by the PRG1, PRG2 and PRG3 facies: PRG1 represents a plagioclase-rich cumulate, PRG2 a differentiated melt, and PRG3 a late residual melt. Mineral assemblages are Pl and subordinate Qtz, Grt, Bt and Ms in PRG1, Pl, Ms, Grt, Qtz±Kfs and major Bt in PRG2, and conspicuous Kfs in PRG3. Remarkably, garnet crystallized throughout the differentiation sequence of the Peñón Rosado granite (SiO_2=65.70–74.57%). Its textural characteristics and chemical compositions indicate that it could have formed by direct nucleation and subsequent crystallization from the peraluminous magma in equilibrium with solid phases such as biotite and white mica. Fractionation of Mn in garnet as well as the proportion of garnet that crystallizes is roughly controlled by the evolving composition of the different granitic facies. Based in our garnet studies we confirm the finding of previous garnet studies from metamorphic and felsic granites, that the zoning in garnet is strongly temperature-dependent. At magmatic temperatures above ~ 700 °C, the diffusion becomes sufficiently rapid to eliminate compositional zoning, typically producing spessartine–almandine garnets that are unzoned or have “spessartine inverse bell-shaped profiles”. Contrarily, garnet housed in granitic rocks, but exhibiting “spessartine bell-shaped profile” must be considered of metamorphic origin (i.e., xenocrystic), or formed in very felsic magmas (SiO_2=73–76%) crystallizing below ~ 700 °C. In these cases geothermobarometric calculation is dangerous and should be used with caution.

The parental magma of the Peñón Rosado granite was derived from a plagioclase-rich metasedimentary source (metagreywacke) in the middle crust (~ 19−20 km) under moderate-low magmatic temperature conditions. The parental magma resulted from H_2O-fluxed melting of metagreywacke, with the heat input coming from a major metaluminous suite that caused local anatexis of the surrounding metasediments.

Acknowledgements

Financial support was provided by IM40 2000 (ANPCyT), BTE2001-1486 (Spain) y PIP02082 CONICET. Juan A. Dahlquist thanks Professor César Casquet and José González del Tánago (UCM) as well as to the technician Alfredo Fernández for their assistance with use of the electron microprobe. The authors thank Professor Edgardo Baldo (CONICET-UNC) by the assistance in P–T calculation using TWQ of Berman (1991), Dr. Raúl Lira (CONICET-UNC) by mineralogical discussion, and Professor Calvin Miller by discussion about T_{Zr} and the occurrence of garnet in igneous rocks. We greatly appreciate the critical comments of two anonymous colleagues and the

valuable suggestions of the Editor Stephen Foley, that led to improvements in the quality of the work. Juan A. Dahlquist thanks CRILAR for general technical support.

References

Allan, B.D., Clarke, D.B., 1981. Occurrences and origin of garnets in the South Mountain Batholith, Nova Scotia. Can. Mineral. 19, 19–24.

Anderson, A.T., 1984. Probable relations between plagioclase zoning and magma dynamics, Fuego Volcano Guatemala. Am. Mineral. 69, 660–676.

Anderson, J.L., 1996. Status of thermobarometry in granitic batholiths. Trans. R. Soc. Edinb. Earth Sci. 87, 125–138.

Atherton, M.P., 1968. The variation in garnet, biotite and chlorite compositions in medium grade pelitic rocks from the Dalradian, Scotland, with particular reference to the zonation in garnet. Contrib. Mineral. Petrol. 18, 347–371.

Arth, J.G., 1976. Behavior of trace elements during magmatic processes — a summary of theoretical models and their applications. J. Res. U.S. Geol. Surv. 4, 41–47.

Barker, F., 1979. Trondhjemite: definition, environment and hypotheses of origin. In: Barker, F. (Ed.), Trondhjemites, Dacites and Related Rock. Elsevier, Amsterdan, pp. 1–12.

Berman, R.G., 1990. Mixing properties of Ca–Mg–Fe–Mn garnets. Am. Mineral. 75, 328–344.

Berman, R.G., 1991. Thermobarometry using multiequilibrium calculations: a new technique with petrologic applications. Can. Mineral. 29, 833–855.

Bohlen, S.R., Montana, A., Kerrick, D.M., 1991. Precise determinations of equilibria kyanite–sillimanite and kyanite–andalusite and revised triple point for Al_2SiO_5 polymorphs. Am. Mineral. 76, 677–680.

Boynton, W.V., 1984. Geochemistry of the rare earth elements: meteorites studies. In: Henderson, P. (Ed.), Rare Earth Element Geochemistry. Elsevier. 63–114 pp.

Bryan, W.B., Finger, L.W., Chayes, F., 1969. Estimating proportions in petrographic mixing equations by least-squares approximation. Science 163, 926–927.

Carr, M.J., 1998. IgPet32 program, Terra Software Inc.

Casquet, C., Baldo, E., Pankhurst, R.J., Rapela, C.W., Galindo, C., Fanning, C.M., Saavedra, J., 2001. Involvement of the Argentine precordillera terrane in the Famatinian moble belt: U–Pb SHRIMP and metamorphic evidence from the Sierra de Pie de Palo. Geology 29, 703–706.

Chappell, B.W., 1997. Compositional variation within granite suites of the Lachlan Fold Blet: its causes and implications for the physical state of granite magma. Trans. R. Soc. Edinb. Earth Sci. 88, 159–170.

Chappell, B.W., White, A.J.R., 1992. I- and S-type granites in the Lachlan Fold Belt. Trans. R. Soc. Edinb. Earth Sci. 83, 1–26.

Clarke, D.B., 1981. The mineralogy of peraluminous granites: a review. Can. Mineral. 19, 3–17.

Clarke, D.B., Dorais, M., Barbarin, B., Barker, D., Cesare, B., Clarke, G., el Baghdadi, M., Erdmann, S., Förster, H.J., Gaeta, M., Gottesmann, B., Jamieson, R.A., Kontak, D.J., Koller, F., Gomes, C.L., London, D., Morgan Vi, G.B., Neves, L.J.P.F., Pattison, D.R.M., Pereira, A.J.S.C., Pichavant, M., Rapela, C.W., Renno, A.D., Richards, S., Roberts, M., Rottura, A., Saavedra, J., Sial, A.N., Toselli, A.J., Ugidos, J.M., Uher, P., Villaseca, C., Visonà, D., Whitney, D.L., Williamson, B., Woodard, H.H., 2005. Occurrence and origin of andalusite in peraluminous felsic igneous rocks. J. Petrol. 46, 441–472.

Clemens, J.D., Wall, V.J., 1981. Origin and crystallization of some peraluminous (S-type) granitic magmas. Can. Mineral. 19, 111–131.

Dahlquist, J.A., 2002. Mafic microgranular enclaves: early segregation from metaluminous magma (Sierra de Chepes), Pampean Ranges, NW Argentina. J. South Am. Earth Sci. 15, 643–655.

Dahlquist, J.A., Galindo, C., 2004. Geoquímica isotópica de los granitoides de la sierra de Chepes: un modelo geotectónico y termal, implicancias para el orógeno famatiniano. Rev. Asoc. Geol. Argent. 59 (1), 57–69.

Dahlquist, J.A., Rapela, C.W., Pankhurst, R.J., Baldo, E., Saavedra, J., Alasino, P.H., 2005a. Los granitoides de la sierra de Chepes y su comparación con granitoides paleozoicos de las Sierras Pampeanas: Implicancias para el orógeno famatiniano. In: Dahlquist, J.A., Baldo, E.G., Alasino, P.H. (Eds.), Geología de la provincia de La Rioja — Precámbrico–Paleozoico Inferior. Asoc. Geol. Argentina, Serie D, Publ. Esp., vol. 8, pp. 87–108.

Dahlquist, J.A., Rapela, C.W., Baldo, E.G., 2005b. Cordierite-bearing S-Type granitoids in the Sierra de Chepes (Sierras Pampeanas): petrogenetic implications. J. South Am. Earth Sci. 20, 231–251.

Dahlquist, J.A., Alasino, P.H., Galindo, C., Pankhurst, R.J., Rapela, C.W., Saavedra, J., Casquet, C., Baldo, E., González Casado, J.M., 2006. Evolución magmática del granito Peñón Rosado, cerro Asperecito, flanco occidental de la sierra de Famatina. Rev. Asoc. Geol. Argent. 61 (1), 93–111.

Dalziel, I.W.D., 1997. Neoproterozoic–Paleozoic geography and tectonic review, hypothesis, environmental speculation. Geol. Soc. Amer. Bull. 109, 16–42.

Debon, F., Le Fort, P., 1983. A chemical–mineralogical classification of common plutonic rocks and associations. Trans. R. Soc. Edinb. Earth Sci. 73, 135–149.

Deer, W.A., Howie, R.A., Zussman, J., 1992. An Introduction to the Rock Forming Minerals, Second Longman Editions. Longman, London, p. 696.

DePaolo, D.J., Linn, A.M., Schubert, G., 1991. The continental crustal age distribution: methods of determining mantle separation ages from Sm–Nd isotopic data and application to the southwestern United States. J. Geophys. Res. 96, 2071–2088.

Droop, G.T.R., 1987. A general equation for estimating Fe^{3+} in ferromagnesian silicates and oxides from microprobe analyses, using stoichiometric criteria. Mineral. Mag. 51, 431–437.

du Bray, E.A., 1988. Garnet compositions and their use as indicators of peraluminous granitoid petrogenesis — southeastern Arabian Shield. Contrib. Mineral. Petrol. 100, 205–212.

du Bray, E.A., 1994. Composition of micas in peraluminous granitoids of the eastern Arabian Shield. Contrib. Mineral. Petrol. 116, 381–397.

Fujimaki, H., Tatsumoto, M., Aoki, K.-i., 1984. Partition coefficients of Hf, Zr, and REE between phenocrysts and groundmasses. J. Geophys. Res. 89, 662–672.

Ganguly, J., Saxena, S.K., 1984. Mixing properties of aluminosilicate garnets: constraints from natural and experimental data, and applications to geothermo-barometry. Am. Mineral. 69, 88–97.

Ghiorso, M.S., Carmichael, I.S.E., 1987. Modeling magmatic systems: petrologic applications. Reviews in mineralogy. Mineral. Soc. Am. 17, 467–499.

Gomes, M.E.P., Neiva, A.M.R., 2005. Geochemistry of granitoids and their minerals from Rebordelo–Agrochao area, northern Portugal. Lithos 85, 235–254.

Gradstein, F., Ogg, J., Smith, A., 2004. A Geologic Time Scale 2004. Cambridge University Press, Cambridge, UK. 589 pp.

Guowei, Xu, Will, T.M., Powell, R.A., 1994. Calculated petrogenetic K_2O–FeO–MgO–Al_2O_3–SiO_2–H_2O, with particular reference to contact metamorphosed pelites. J. Metamorph. Geol. 12, 99–119.

Hanson, G.N., 1978. The application of trace elements to the petrogenesis of igneous rocks of granite composition. Earth Planet. Sci. Lett. 38, 26–43.

Harrison, T.N., 1988. Magmatic garnets in the Cairngorm granite, Scotland. Mineral. Mag. 52, 659–667.

Hogan, J.P., 1996. Insights from igneous reaction space: a holistic approach to granite crystallization. Trans. R. Soc. Edinb. Earth Sci. 87, 147–157.

Hoisch, T.D., 1990. Empirical calibration of six geobarometers for the mineral assemblage quartz+muscovite+biotite+plagioclase+garnet. Contrib. Mineral. Petrol. 104, 225–234.

Hollister, L.S., 1966. Garnet zoning: an interpretation based on the Rayleigh fractionation model. Science 154, 1647–1651.

Holtz, F., Johannes, W., 1991. Genesis of peraluminous granites I. Experimental investigation of melt composition at 3 and 5 kb and various H_2O activities. J. Petrol. 32, 935–958.

Jarosewich, E.J., Nelen, J.A., Norberg, J.A, 1980. Reference samples for electron microprobe analysis. Geostand. Newsl. 4, 43–47.

Johannes, W., Ehlers, C., Kriegsman, L.M., Mengel, K., 2003. The link between migmatites and S-type granites in the Turku area, southern Finland. Lithos 68, 69–90.

Jordan, T.E., Allmendiger, R.W., 1986. The Sierras Pampeanas of Argentina: a modern analogue of Rocky Mountain foreland deformation. Am. J. Sci. 286, 737–764.

Kebede, T., Koeberl, C., Koller, F., 2001. Magmatic evolution of the Suqii–Wagga garnet-bearing two-mica granite, Wallagga area, western Ethiopia. J. Afr. Earth Sci. 32, 193–221.

Kretz, R., 1983. Symbols for rock-forming minerals. Am. Mineral. 68, 277–279.

Leake, B.E., 1967. Zoned garnets from the Galway granite and its aplites. Earth Planet. Sci. Lett. 3, 311–316.

Manning, D.A.C., 1983. Chemical variation in garnets from aplites and pegmatites, peninsular Thailand. Mineral. Mag. 47, 353–358.

McCarthy, T.S., Groves, D.I., 1979. The Blue Tier Batholith, northeastern Tasmania: a cumulate-like product of fractional crystallization. Contrib. Mineral. Petrol. 71, 193–209.

McCarthy, T.S., Robb, L.J., 1978. On the relationships between cumulus mineralogy and trace and alkalis element chemistry in a Archean granite from Barbeton region, South Africa. Geochim. Cosmochim. Acta 42, 21–26.

McGuire, A.V., Francis, C.A., Diar, M.D., 1992. Mineral standards for electron microprobe analysis of oxygen. Am. Mineral. 77, 1087–1091.

McMullin, D., Berman, R.G., Greenwood, H.J., 1991. Calibration of the SGAM thermobarometer for pelitic rocks using data from phase equilibrium experiments and natural assemblages. Can. Mineral. 29, 889–908.

Miller, C.F., Stoddard, E.F., 1981. The role of manganese in the paragenesis of magmatic garnet: an example from the Old Woman Piute Range, California. J. Geol. 89, 233–246.

Miller, C.F., Stoddard, E.F., Bradfish, L.J., Dollase, W.A., 1981. Composition of plutonic muscovite: genetic implications. Can. Mineral. 19, 25–34.

Miller, C.F., McDowell, S.M., Mapes, R.W., 2003. Hot and cold granites? Implications of zircon saturation temperatures and preservation of inheritance. Geology 31, 529–532.

Nagasawa, H., Schnetzler, C.C., 1971. Partitioning of rare earth, alkali and alkaline earth elements between phenocrysts and acidic igneous magma. Geochim. Cosmochim. Acta 35, 953–968.

Nakamura, N., 1974. Determination of REE, Ba, Fe, Mg, Na and K in carbonaceous and ordinary chondrites. Geochim. Cosmochim. Acta 38, 757–775.

Nash, W.P., Crecraft, H.R., 1985. Partition coefficients for trace elements in silicic magmas. Geochim. Cosmochim. Acta 49, 2309–2322.

Pankhurst, R.J., Rapela, C.W., Saavedra, J., Baldo, E., Dahlquist, J., Pascua, I., Fanning, C.M., 1998. The Famatinian magmatic arc in the central Sierras Pampeanas: an Early to Mid-Ordovician continental arc on the Gondwana margin. In: Pankhurst, R.J., Rapela, C.W. (Eds.), The Proto-Andean Margin of Gondwana. Geol. Soc. (London), Special Publications, vol. 142, pp. 343–367.

Pankhurst, R.J., Rapela, C.W., Fanning, C.M., 2000. Age and origin of coeval TTG, I- and S-type granites in the Famatinian Belt of NW Argentina. Trans. R. Soc. Edinb. Earth Sci. 91, 151–168.

Patiño Douce, A.E., 1996. Effects of pressure and H_2O content on the compositions of primary crustal melts. Trans. R. Soc. Edinb. Earth Sci. 87, 11–21.

Patiño Douce, A.E., Beard, J.S., 1996. Effects of P, $f(O_2)$ and Mg/Fe ratios on dehydration melting of model metagreywackes. J. Petrol. 37, 999–1024.

Patiño Douce, A.E., Harris, N., 1998. Experimental constraints on Himalayan anatexis. J. Petrol. 39, 689–710.

Pattison, D.R.M., Tracy, R.J., 1991. Phase equilibria and thermobarometry of metapelites. In: Kerrick, D.M. (Ed.), Contact Metamorphism. Reviews in Mineralogy. Mineral. Soc. Am., vol. 26, pp. 105–206.

Rapela, C.W., Shaw, D.M., 1979. Trace and major element models of granitoid genesis in the Pampean Ranges, Argentina. Geochim. Cosmochim. Acta 43, 1117–1129.

Rapela, C.W., Pankhurst, R.J., Casquet, C., Baldo, E., Saavedra, J., Galindo, C., Fanning, C.M., 1998a. The Pampean Orogeny of the southern proto-Andes: evidence for Cambrian continental collision in the Sierras de Córdoba. In: Pankhurst, R.J., Rapela, C.W. (Eds.), The Proto-Andean Margin of Gondwana. Geol. Soc. (London), Special Publication, vol. 142, pp. 181–217.

Rapela, C.W., Pankhurst, R.J., Casquet, C., Baldo, E., Saavedra, J., Galindo, C., 1998b. Early evolution of the proto-Andean margin of South America. Geology 26, 707–710.

Richard, L.R., 1995. Mineralogical and petrological, data processing system for Windows, version 2.02. Minpet Geological Software-Logiciel Géologique Minpet, Quebec.

Rollinson, H.R., 1993. Using geochemical data: evaluation, presentation, interpretation. Longman Scientific & Technical Editions, Singapore, p. 352.

Sawyer, E.W., 1987. The role of partial melting and fractional crystallization in determining discordant migmatite leucosome compositions. J. Petrol. 28, 445–473.

Sims, J.P., Ireland, T.R., Camacho, A., Lyons, P., Pieters, P.E., Skirrow, R.G., Stuart-Smith, P.G., 1998. U–Pb, Th–Pb and Ar–Ar geochronology from the southern Sierras Pampeanas, Argentina: implications for the Palaeozoic tectonic evolution of the western Gondwana margin. In: Pankhurst, R.J., Rapela, C.W. (Eds.), The Proto-Andean Margin of Gondwana. Geol. Soc. (London), Special Publication, vol. 142, pp. 259–281.

Spear, F.S., 1993. Metamorphic phases equilibria and pressure–temperature–time paths. Mineral. Soc. Am., Monogr. 1, 779 Washington, USA.

Speer, J.A., 1984. Micas in igneous rocks. Reviews in mineralogy. Mineral. Soc. Am. 13, 357–368.

Steiger, R.H., Jäger, E., 1977. Subcommision of geochronology: convention on the use of decay constants in geo- and chosmochronology. Earth Planet. Sci. Lett. 1, 369–371.

Streckeisen, A., 1976. To each plutonic rock its proper name. Earth. Sci. Rev. 12, 1–33.
Sylvester, P.J., 1998. Post-collisional strongly peraluminous granites. Lithos 45, 29–44.
Tera, F., Wasserburg, G., 1972. U–Th–Pb systematics in three Apollo 14 basalts and the problem of initial Pb in lunar rocks. Earth Planet. Sci. Lett. 14, 281–304.
Thomas, W.A., Astini, R.A., 1996. The Argentine precordillera: a traveller from the Quachita embayment of North America Laurentia. Science 273, 752–757.
Vance, J.A., 1962. Zoning in igneous plagioclase: normal and oscillatory zoning. Am. J. Sci. 260, 746–760.
Vernon, R.H., Richards, S.W., Collins, W.J., 2001. Migmatite–granite relationships: origin the Cooma Granodiorite magma, Lachlan Fold Belt, Australia. Phys. Chem., Earth (A) 26, 267–271.
Vielzeuf, D., Holloway, J.R., 1988. Experimental determination of the fluid-absent melting relations in the pelitic system. Contrib. Mineral. Petrol. 98, 257–276.
Villaseca, C., Barbero, L., Herreros, V., 1998. A re-examination of the typology of peraluminous granite types in intracontinental orogenic belts. Trans. R. Soc. Edinb. Earth Sci. 89, 113–119.
Walker, J.A., Carr, M.J., 1986. Compositional variations caused by phenocryst sorting at Cerro Negro volcano, Nicaragua. Geol. Soc. Amer. Bull. 97, 1156–1162.
Williams, I.S., 1998. U–Th–Pb geochronology by ion microprobe. In: McKibben, M.A., Shanks, W.C. (Eds.), Applications of Micro-analytical Techniques to Understanding Mineralising Processes. Rev. Econ. Geol., vol. 7, pp. 1–35.
Wyborn, D., Turner, B.S., Chappell, B.W., 1987. The Boggy Plain supersuite: a distinctive belt of I-type igneous rocks of potential economic significance in the Lachlan Fold Belt. Aust. J. Earth Sci. 34, 21–43.
Yardley, B.W.D., 1977. An empirical study of diffusion in garnet. Am. Mineral. 62, 793–800.